Uncertainty in gap filling and estimating the annual sum of carbon dioxide exchange for the desert Tugai forest, Ebinur Lake Basin, Northwest China

Dexiong Teng [1, 2] , **Xuemin He** [1, 2] , **Jingzhe Wang** [1, 2] , **Jinlong Wang** [1, 2] , **Guanghui Lv** [Corresp. 1, 2]

1 College of Resources and Environment Science, Xinjiang University, Urumqi, Xinjiang, China

2 Key Laboratory of Oasis Ecology of Ministry of Education, Xinjiang University, Urumqi, Xinjiang, China

Corresponding Author: Guanghui Lv
Email address: Guanghui_xju@sina.com

In most eddy covariance studies, carbon flux measurements have a high defect rate for a variety of reasons. Obtaining the annual sum of carbon dioxide exchange requires imputation of data gaps with high precision and accuracy. This study used five methods to fill the gaps in carbon flux data and estimate the total annual carbon dioxide exchange of the Tugai forest in the arid desert ecosystem of Ebinur Lake Basin, Northwest China. The Monte Carlo method was used to estimate the random error and bias caused by gap filling. The results revealed that (1) there was a seasonal difference in the friction velocity threshold of nighttime flux, with values in the growing season and non-growing season of 0.12 and 0.10 m/s, respectively; (2) the five gap-filling methods explained 77%–84% of the data variability in the fluxes, and the random errors estimated by these methods were characterized by non-normality and leptokurtic heavy tail features, following the Laplacian (or double-exponential) distribution; (3) estimates of the annual sum of carbon dioxide exchange using the five methods at the study site in 2015 ranged from -178.25 to -155.21 g C m^{-2} yr^{-1}, indicating that the Tugai forest in the Ebinur Lake Basin is a net carbon sink. The standard deviation of the total annual carbon dioxide exchange sums estimated by the five different methods ranged from 3.15 to 19.08 g C m^{-2} yr^{-1}, with bias errors ranging from -13.69 to 14.05 g C m^{-2} yr^{-1}. This study provides a theoretical basis for the carbon dioxide exchange and carbon source/sink assessment of the Tugai forest in an arid desert ecosystem. In order to explore the functioning of the Tugai forest at this site, a greater understanding of the underlying ecological mechanisms is necessary.

1   **Uncertainty in gap filling and estimating the annual sum of carbon dioxide exchange for the**
2   **desert Tugai forest, Ebinur Lake Basin, Northwest China**

3   Dexiong Teng [1,2], Xuemin He[1,2], Jingzhe Wang [1,2], Jinlong Wang[1,2], Guanghui Lv[1,2*]
4   [1] College of Resources and Environment Science, Xinjiang University, Urumqi, Xinjiang, China;
5   [2] Key Laboratory of Oasis Ecology of Ministry of Education, Xinjiang University, Urumqi,
6   Xinjiang, China
7   Corresponding Author: Guanghui Lv
8   Email address: ler@xju.edu.cn.

10 **Abstract:** In most eddy covariance studies, carbon flux measurements have a high defect rate for
11 a variety of reasons. Obtaining the annual sum of carbon dioxide exchange requires imputation of
12 data gaps with high precision and accuracy. This study used five methods to fill the gaps in carbon
13 flux data and estimate the total annual carbon dioxide exchange of the Tugai forest in the arid
14 desert ecosystem of Ebinur Lake Basin, Northwest China. The Monte Carlo method was used to
15 estimate the random error and bias caused by gap filling. The results revealed that (1) there was a
16 seasonal difference in the friction velocity threshold of nighttime flux, with values in the growing
17 season and non-growing season of 0.12 and 0.10 m/s, respectively; (2) the five gap-filling methods
18 explained 77%–84% of the data variability in the fluxes, and the random errors estimated by these
19 methods were characterized by non-normality and leptokurtic heavy tail features, following the
20 Laplacian (or double-exponential) distribution; (3) estimates of the annual sum of carbon dioxide
21 exchange using the five methods at the study site in 2015 ranged from -178.25 to -155.21 g C m^{-2}
22 yr^{-1}, indicating that the Tugai forest in the Ebinur Lake Basin is a net carbon sink. The standard
23 deviation of the total annual carbon dioxide exchange sums estimated by the five different methods
24 ranged from 3.15 to 19.08 g C m^{-2} yr^{-1}, with bias errors ranging from -13.69 to 14.05 g C m^{-2} yr^{-1}.
25 This study provides a theoretical basis for the carbon dioxide exchange and carbon source/sink
26 assessment of the Tugai forest in an arid desert ecosystem. In order to explore the functioning of
27 the Tugai forest at this site, a greater understanding of the underlying ecological mechanisms is
28 necessary.

1. Introduction

30 In recent decades, with the development of sonic anemometers, the eddy covariance method
31 has become one of the direct techniques for determining the surface–atmosphere carbon dioxide
32 exchange (Baldocchi, 2014). This method consists of calculating the covariance of fluctuations in
33 vertical wind speed and gas concentration, providing valuable data on the dynamic interactions of
34 the surface and atmosphere. At present, more than 800 eddy covariance stations around the world
35 are monitoring the carbon dioxide and water exchange of the surface–atmosphere. These stations
36 are located in forests, grasslands, farmlands, and other terrestrial ecosystems, concentrated in the
37 grasslands of North America, Europe, and Africa, as well as in forest ecosystems (Baldocchi et al.,
38 2018; Rebane et al., 2019). However, there have been few consecutive observations of material
39 fluxes in arid desert ecosystems, leading to great difficulties in understanding the role of arid desert
40 ecosystems in the global carbon cycle.
41 Eddy covariance (EC) is influenced by numerous factors during the measurement of carbon
42 dioxide (CO_2) flux (e.g., limited turbulence, non-stationarity, blizzards, sand, precipitation, and
43 instrument resolution), usually resulting in data loss or abnormalities. One study found that missing
44 or abnormal data in carbon flux observations account for approximately 20%–60% of the total
45 (Papale et al., 2006). This poses enormous difficulties for estimating the annual sum of carbon
46 dioxide exchange. The important step in this estimation is gap filling. To solve this problem, a
47 number of approaches have been proposed, including non-linear regression, look-up tables, mean
48 diurnal variation methods (Falge et al., 2001), artificial neural networks (Braswell et al., 2005;
49 Moffat et al., 2007; Papale and Valentini, 2003), marginal distribution sampling (Reichstein et al.,
50 2005), data assimilation, and Bayesian model approaches (Gove and Hollinger, 2006). The

51 differences among gap-filling methods for missing data and their impacts on the estimation of
52 carbon dioxide exchange vary temporally and spatially in urban, forest, and grassland ecosystems
53 (Kunwor et al., 2017; Liu et al., 2010; Moffat et al., 2007). Establishing a standard set of gap-
54 filling methods can enhance comparability between different sites in regional and global flux
55 networks (Falge et al., 2001). Models based on the light and temperature response are widely used
56 for filling gaps in carbon flux observations of natural vegetation (Desai et al., 2005). Gap-filling
57 approaches that rely on the average temperature underestimate flux values compared to those that
58 preserve the observed variance as a consequence of Jensen's inequality, adding further bias to the
59 long-term estimates of carbon dioxide exchange (Moffat et al., 2007). The introduction of
60 additional predictors, such as vapor pressure deficit and soil moisture content, may reduce the bias
61 that has been found to be proportional to the percentage of gaps filled in the annual sums of carbon
62 dioxide exchange (Falge et al., 2001). Hagen et al. (2006) utilized two regression models to fill the
63 gaps of carbon dioxide exchange in Howland Forest, Maine, USA, concluding that the greatest
64 uncertainty comes from model differences. The Gaussian processes model and the radial basis
65 function neural network have been shown to significantly improve model performance by
66 capturing complex relationships in carbon dioxide exchange studies (Menzer et al., 2013; Menzer
67 et al., 2015; Schmidt et al., 2007). There have been few studies on gap filling and the annual sum
68 of carbon dioxide exchange in arid desert ecosystems, and uncertainty still remains in the
69 estimation and evaluation of the annual sum of carbon dioxide exchange (Soloway et al., 2017).
70 The evaluation of gap-filling uncertainty plays an important role in estimating regional carbon sink
71 strength. The scientific comparison and evaluation of carbon flux gap-filling and the carbon budget
72 in arid desert ecosystems are conducive to the sharing of flux data and its related research.

73   Arid desert ecosystems are playing an increasingly important role in the global carbon cycle
74 (Donohue et al., 2013) and may even supplant tropical rainforests, affecting the interannual
75 variation in the global carbon cycle (Poulter et al., 2014). Recent findings that desert regions
76 remove carbon dioxide from the atmosphere at a magnitude of ~100 g C m^{-2} yr^{-1} suggest that these
77 systems may explain at least a portion of the terrestrial carbon sink that has not been fully identified
78 nor had its mechanisms explained in the global carbon cycle (Jasoni et al., 2005; Ma et al., 2014;
79 Stone, 2008; Wohlfahrt et al., 2008; Xie et al., 2009). Irrigated saline/alkaline arid land is a
80 potentially large carbon sink in the terrestrial ecosystem (Li et al., 2015). The study of carbon flux
81 has direct implications for the missing global carbon sink. The Ebinur Lake Basin is a typical
82 salinized area (Wang et al., 2019b). The Tugai forest is the only natural forest community in the
83 Ebinur Lake Basin, and its contribution to the carbon dioxide exchange of the region cannot be
84 overlooked. Estimating the annual sum of the carbon dioxide exchange of the Tugai forest can
85 provide insight into the issue of the missing carbon sink to a certain extent.

86   In this study, EC techniques were used to obtain continuous records of the carbon flux of the
87 Tugai forest on the northern bank of the Aqikesu River in the Ebinur Lake Wetland National
88 Nature Reserve, Northwest China. We evaluated the ability of five gap-filling methods to analyze
89 random uncertainties and bias in order to provide more robust estimations of the annual sums of
90 the carbon dioxide exchange from the Tugai forest. In addition, the impacts of these different gap-
91 filling methods—the artificial neural network for backward propagation algorithm (ANN), the

92   radial basis function (RBF) neural network, the Gaussian processes model (GP), the regularized
93   hierarchical linear model (HLM) with a Bayesian framework, and marginal distribution sampling
94   (MDS)—on the annual carbon dioxide exchange in the Tugai forest were examined and the
95   random uncertainties were studied.

2. Materials and Methods

2.1 Site description

98   The study site is located in the Ebinur Lake Wetland National Nature Reserve in the Bortala
99   Mongolian Autonomous Prefecture of the Xinjiang Uygur Autonomous Region, Northwest China
100 (44°37′05″–45°10′35″N, 82°30′47″–83°50′21″E). The Xinjiang Ebinur Lake Wetland National
101 Natural Protection Zone Management Bureau approved site access. With a temperate continental
102 climate, the reserve located in the Alataw Pass (Fig. 1a) is a typical arid desert, featuring high
103 temperatures, drought, and sufficient sunshine in summer, and dry and cold conditions in winter.
104 With strong winds from the Alataw Mountain Pass, the loose and relatively thick Quaternary
105 sediment provides a rich sand source for sand shifting, and the soil salinization is generally
106 pronounced. Typical soils in the study area are gray desert soil, gray-brown desert soil, and aeolian
107 sandy soil. The azonal soil is dominated by saline soil, and supplemented by meadow soil, bog
108 soil, and brown calcic soil (Jin et al., 2010; Wang et al., 2019a). The annual average temperature
109 in the basin is 6–8°C, the annual precipitation is approximately 100 mm, and the annual average
110 sunshine is 2,800 h. The ecological environment is relatively fragile and consists primarily of two
111 ecological ecosystems: the wetland ecosystem and the arid grassland–forest ecosystem (Fig. 1b).
112 The flux observation tower stands near the Aqikesu River (44°37′4.8″N, 83°33′59.4″E) in the
113 forest-desert transitional zone influenced by lakes and rivers (Fig. 1e). The dominant species of
114 plants in this region are *Populus euphratica*, *Haloxylon ammodendron*, and *Phragmites australis*,
115 with a combined coverage of more than 60%, accompanied by a variety of shrubs, herbs, and
116 desert-specific short-lived plants (He et al., 2014; He et al., 2015; Wang et al., 2019). During the
117 observation period, the annual average temperature at the flux tower was 9°C, the highest
118 temperature was 43°C, and the lowest temperature was -26°C. More weather conditions are shown
119 in Fig. 2.

120 **Fig. 1.** Aerial photograph of the tower site

121 (a) Location map of the Ebinur Lake Basin, (b) Location map of the measurement tower, (c)
122 aerial photo of the tower site in August (Photograph credit: Jinlong Wang), (d) photograph of
123 the tower site in May (Photograph credit: Dexiong Teng), and (e) remote sensing image in
124 June and the average footprint for the entire observation period (Kormann and Meixner, 2001).
125 The measurement tower is marked with a red circle. The white lines represent isopleths of the
126 average contributions.

127 **Fig. 2.** Meteorological observations during the year of measurement

128 Half-hour averaged values of (a) air temperature (T_{air}), (b) precipitation, (c) global radiation

129   (Rg), (d) wind speed, and (e) relative humidity (RH) during the observation period

130 *2.2 Carbon flux data observation and processing*

131   The data for this study were obtained from the Ebinur Lake Desert Ecosystem Flux Tower
132 (2012XJ-AibiHu-OPEC) using an eddy covariance system consisting of a 3-D sonic anemometer
133 (CSAT3, Campbell Scientific, USA) and an open-path infrared gas analyzer (EC150, Campbell
134 Scientific, USA). The instruments were installed on the southwest side of the tower above the
135 forest canopy at a height of 15.0 m (~4.0 m above the mean canopy height). Total CO_2 fluxes were
136 measured from January 1, 2015 to December 31, 2015. Using EddyPro 6.2.1 software, 30-min
137 averaged values were calculated, resulting in 17,520 observations (Table 1). Webb, Pearman, and
138 Leuning (WPL) correction was used during the data pre-processing (Webb et al., 2010). Due to
139 extremely low temperatures and instrument failure, 4,858 (approximately 27.73%) of the data
140 observations were missing. Based on the stationarity test (Foken and Wichura, 1996; Mauder et
141 al., 2013), the observations were divided into 3 quality classes (0, 1, and 2). Only high-quality data
142 were selected to establish the model, and 5,784 (approximately 33.01%) of the data observations
143 with a rank other than 0 were excluded. Based on changes in surface vegetation, the year can be
144 divided into the growing season (May–September) (Munir et al., 2015) and the non-growing
145 season (January–April and October–December). This study divided the data into daytime and
146 nighttime periods based on the sunrise and sunset times at the location of the flux tower. The
147 observation time of the daytime data extended from sunrise to sunset, and the observation time of
148 the nighttime data extended from sunset to sunrise. There were 8,924 daytime observations,
149 accounting for 50.94% of the total and 8,596 nighttime observations, accounting for 49.06%. The
150 total count of null and low-quality observations was 6,735, accounting for 38.44%. Thus, there
151 was a large amount of missing data, and data gap-filling faced enormous challenges.

152   Corresponding to the 30-min carbon dioxide flux (F_C) observation data, eight explanatory
153 variables, including soil temperature, air temperature, relative humidity, incident radiation,
154 scattered radiation, saturated vapor pressure deficit, normalized difference vegetation index
155 (NDVI), and water vapor partial pressure, were selected as the driving factors for the gap-filling
156 models. Partial explanatory variables needed to be converted (Table 1). The selected
157 meteorological variables were normalized by mapping all explanatory variables to (0, 1) via linear
158 transformation and using the 2 variables of growing and non-growing to describe the season, both
159 of which are binary (0 or 1). Based on the sunrise and sunset times, the data were classified into 2
160 types, daytime and nighttime, which were represented by binary variables. The observation data
161 were divided into 3 parts: high-quality data used for training and testing models; data used to
162 calculate the annual exchange of carbon flux; and gaps.

163   **Table 1.** Data source of the driving factors and their corresponding pre-processing

164 *2.3 Net ecosystem carbon dioxide exchange*

165   The net ecosystem carbon dioxide exchange (NEE) between the ecosystem and the
166 atmosphere can be estimated as the sum of the vertical eddy covariance and the storage term:

$$NEE = F_C + F_S \tag{1}$$

168   The low density of the Tugai forest canopies, which is favorable to eddy penetration, can
169   reduce the importance and frequency of storage events. The lower the vegetation height, the less
170   storage of CO_2. In addition, the effect of the storage terms on the carbon uptake characteristics
171   over long-term time scales is not significant since the cumulative value of the storage terms in the
172   long-term is approximately equal to 0 (Massman and Lee, 2002). In this study, the storage terms
173   were considered to be negligible compared with the terms associated with eddy covariance
174   fluctuation.

175   *2.4 Night friction velocity threshold*

176   The friction velocity u^* is intended to capture the turbulence characteristics in the vicinity of
177   the surface. In a general way, u^* can be expressed as a fraction of the average wind speed u:

$$u^* \approx \frac{u}{\Pi}, \tag{2}$$

179   where the parameter Π is the roughness index. We used standardized major axis (SMA) regression
180   to compare the roughness difference between the growing season and the non-growing season
181   (Warton et al., 2012).
182   Due to the relatively stable atmospheric stratification at night, the carbon flux observed using
183   eddy covariance techniques cannot truly represent the surface–atmosphere carbon dioxide
184   exchange. Nighttime data processing was an important step in the flux data processing. The
185   uncertainty of the annual sum of ecosystem carbon exchange caused by different treatment
186   methods can reach 150 g C m^{-2} yr^{-1} (Williams et al., 2009). The bias due to the data processing
187   methods in this study area, as well as the estimated bias from the gap-filling techniques, may be
188   greater. To correct selective systematic errors, the international flux community usually excludes
189   nighttime observations below the friction velocity threshold in order to ensure that eddy covariance
190   techniques are measured under strong turbulence conditions (Aubinet and Feigenwinter, 2010).
191   Currently, despite theoretical and practical deficiencies, the empirical and effective method for
192   processing nighttime negative flux is filtered by the friction velocity threshold (Aubinet and
193   Feigenwinter, 2010). The friction velocity threshold can be determined by testing the relationship
194   between the flux and the friction velocity, since, in theory, carbon dioxide flux and friction velocity
195   are independent. When the friction velocity is lower than this threshold, F_C decreases as the friction
196   velocity decreases. The nighttime flux data of the growing and non-growing seasons were sorted
197   based on the increment of u^*, and the friction velocity thresholds for the growing and non-growing
198   seasons were then determined. A total of 45 levels were set, and the thresholds were derived by
199   statistically comparing (using the two-sample Wilcoxon test) the flux average at each u^* level with
200   the flux average at the next higher u^* level.

201   *2.5 Detection of abnormal data points*

202   The technique of using eddy covariance to observe carbon flux is susceptible to
203   environmental factors such as rapid changes in turbulence, as well as the instrumentation itself.

204   The 30-min data obtained from processing the observed raw data contained a large number of gaps
205   and abnormal values, which deviated from the range of normal data variation (Li et al., 2005).
206   Given the relatively clear daily variation of the carbon flux data, this study divided the carbon flux
207   data into 48 parts according to the time of day and defined any carbon flux data beyond the upper
208   and lower limits as abnormal points. For outliers in the continuous data, this study used 7 days as
209   the window to determine the difference between the median of 3 consecutive data points (D_i). The
210   specific algorithm (Papale et al., 2006) was as follows:

$$D_i = (F_{Ci} - F_{Ci-1}) - (F_{Ci+1} - F_{Ci}), \tag{3}$$

212   where F_C is the carbon dioxide flux, and i is the ordinal number of the observation data for 30 min.
213   When D_i satisfies the relationship

$$Md + (z * MAD/0.6745) > D_i > Md - (z * MAD/0.6745), \tag{4}$$

215   the corresponding i^{th} observation data point is normal; otherwise, it is defined as an "abnormal
216   point" and is eliminated. (Daytime and nighttime data were processed separately.) Md is the
217   median of the F_C differences between all sets of two adjacent points. MAD = median ($|D_i - Md|$)
218   and is the median of all $|D_i - Md|$ for a 7-day window. In this study, the sensitivity coefficient z of
219   the artificially defined outlier identification was set to 5.5.

220   *2.6 Gap-filling methods*

221   Given the actual conditions of a site, selecting the appropriate flux data processing method
222   and reducing the uncertainty of the flux data estimation are important issues that need to be
223   understood and analyzed by the flux community. The effectiveness of different methods for filling
224   gaps in carbon dioxide flux (F_C) data has been investigated. This study used ANN, RBF, GP, HLM,
225   and MDS to fill the gaps. The high-quality data were randomly divided into 2 parts, 80% of which
226   were used to train the model and 20% to test the model. In order to avoid overfitting, 4 different
227   methods (ANN, GP, HLM, and RBF) were used for model training before the best model for each
228   method was selected and used for prediction. In the data analysis, the neuralnet, RSNNS, laGP,
229   and INLA packages (R language) were used to train and test ANN, RBF, GP, and HLM,
230   respectively. The gap-filling model was evaluated in terms of 3 statistical factors: the coefficient
231   of determination (R^2), root mean square error (RMSE), and bias error (BE).

232   *2.6.1 ANN and RBF*

233   For artificial neural network training, the input data were passed through the nodes using
234   weighted connections, the error between the predicted and actual output values was calculated by
235   backpropagation, and the weight was adjusted to minimize the error (Braswell et al., 2005; Papale
236   and Valentini, 2003). The training data were pre-sampled to ensure equal coverage under different
237   conditions, and fuzzy values were used to represent additional information such as time (Moffat
238   et al., 2007; Papale and Valentini, 2003). By testing the structure of the artificial neural network,
239   the network was built to be as simple as possible, and overfitting was avoided.
240   During the model training process, with the exception of the input and output layers, only 1
241   hidden layer was needed to obtain sufficient results; additional hidden layers did not improve
242   model performance. In the output layer, a linear transfer function was used. Both the ANN and

243   RBF were built using the input variables listed in Table 1, as well as the 30-min data points of F_C,
244   with the same parameters presented by Schmidt et al., 2007. The number of neurons in the ANN
245   hidden layer was 5, and the number of neurons in the RBF hidden layer was 181.

246   *2.6.2 Regularized hierarchical linear regression model with Bayesian framework*

247   Since signals may be less pronounced than random errors, overfitting is a potential problem
248   in regression models in which parameters estimate noise rather than the underlying signal. In
249   earlier works, hierarchical modeling produced more accurate predictions than regular regression
250   and also tended to reduce overfitting in the presence of a hierarchical data structure (Gelman,
251   2006). There have been some detailed examples highlighting uses of Bayesian and hierarchical
252   Bayesian methods in plant physiology and ecosystem ecology (Ogle and Barber, 2008).
253   Hierarchical modeling has been proposed to predict monthly streamflow (Lima and Lall, 2010)
254   and extreme flooding (Lima et al., 2016). This study used varying intercepts of hierarchical
255   modeling for the carbon flux data with a temporally hierarchical structure. The form of the model
256   was as follows:

257
$$y_{ij} \sim N\left(\alpha_j + \beta x_{ij}, \sigma_y^2\right), \text{for } i = 1,\ldots,365; j = 1,\ldots,48, \quad (5)$$

258
$$\alpha_j \sim N\left(\gamma_j, \sigma_{\alpha_j}^2\right), \quad (6)$$

259
$$\beta | \sigma_\beta^2 \sim N\left(0, \sigma_\beta^2 I\right), \quad (7)$$

260   where y_{ij} is F_C at time j within Julian Day i, and x_{ij} is a vector for the environmental measurement
261   (Table 1) corresponding to F_C. The hyperparameters of the prior distribution of α_j are γ_j and $\sigma_{\alpha_j}^2$.

262   In previous studies, the prior ridge has been chosen for shrinking coefficients due to its weaker

263   penalization of large coefficients (Fahrmeir et al., 2009). Therefore, we assumed that $\beta | \sigma_\beta^2 \sim N$ (0,

264    $\sigma_\beta^2 I$).

265   *2.6.3 Gaussian processes*

266   As nonlinear regression tools, Gaussian processes have nonparametric flexibility and can be
267   used to fit arbitrary functions or surfaces (Azmy et al., 2009). Therefore, the Gaussian process is
268   often used to replace the supervised neural network in nonlinear regression. The GP can be
269   described by a mean function $m(x)$ (a vector) and a covariance function $k(x, x')$ (a matrix):
270
$$f(x) = GP(m(x), k(x, x')), \quad (8)$$
271   where $f(x)$ is a random variable. In this study, $f(x)$ was the modeled F_C. This assumes that the
272   mean function $m(x)$ is equal to 0 since our data were standard normalized, and $k(x, x')$ is a function
273   of the Euclidean distance between the predictors x and x'. The squared exponential covariance
274   function was chosen with automatic relevance determination (Bishop, 2006):

275
$$\text{cov}(f(x), f(x')) = k(x, x') = \sigma_f^2 \exp\left(-\frac{1}{2}\Sigma_{i=1}^{D} \frac{\|x_i - x_i'\|}{\sigma_i^2}\right), \qquad (9)$$

276 where σ_f^2 is a hyperparameter for the amplitude variance. The width hyperparameter σ_i^2 is separate

277 for each input variable x_i.

2.7 Characteristics of random uncertainty

279   The correlation between the predicted carbon flux and its corresponding residual is
280 represented by Kendall's tau (τ) coefficient. If τ is close to 0, the posterior residual does not
281 contain structural error from the model. Conversely, if τ is close to 1, the predicted value should
282 contain the model structure error of the influence, and such interpretation information may be
283 passed to the posterior residual (Wang et al., 2015).
284   The relationship between the standard deviation of the random uncertainty of carbon flux
285 observations and the magnitude of the observed values is commonly expressed as follows:

286
$$\sigma(\varepsilon) = a + b|F_c|. \qquad (10)$$

287 The intercept term a varies from site to site, with a typical range of 0.9–3.5 μmol m^{-2} s^{-1}
288 (Richardson et al., 2008). The larger the value of a, the greater the uncertainty. The range of the
289 slope b is usually 0.1–0.2; the smaller the value of b, the closer the probability distribution of the
290 uncertainty to white noise.

2.8 Uncertainty in the cumulative carbon dioxide exchange

292   To determine the random error of carbon flux and the error caused by interpolation, this study
293 used the bootstrap method to estimate the deviation of the annual sum of ecosystem carbon
294 exchange and its 95% confidence interval. Estimating the root mean square error (RMSE),
295 variance, and bias of the annual sum of carbon exchange required a complete carbon flux time
296 series (1,000 bootstrap sequences). The variance of the total annual carbon exchange can be
297 directly estimated, but due to vacancies in the carbon flux data, the deviation of the total annual
298 carbon exchange cannot be directly estimated. To estimate the (potential) bias in carbon flux
299 vacancy data, we used the bootstrap method to simulate and analyze the bias of high-quality
300 modeling data in order to extend it to an annual scale (Richardson et al., 2006; Wang et al., 2015).
301 The estimation steps used to determine the bias of the annual sum of carbon exchange were as
302 follows:
303 (1) The vector $\hat{\varepsilon}$, which is the estimation of the random error ε, was estimated by subtracting the
304 observed F_C from the F_C estimated by the models.
305 (2) All data (observed F_C with gaps as well as modeled F_C) were divided in terms of the growing
306 season, daytime, non-growing season, and nighttime. The daytime data of the growing season were
307 divided according to the incident radiation intensity (limited to 400 W·m^{-2}), resulting in 6 parts.
308 (3) $\hat{\varepsilon}$ was repeatedly sampled in order to obtain a new complete bias sequence (a total of 17,520
309 repeated extractions per year).
310 (4) A cumulated summation of the new complete bias sequence was calculated.

311   (5) Steps (3) and (4) were repeated 1,000 times.
312   (6) The empirical distribution of the 1,000 biases of the annual sum of ecosystem carbon exchange,
313   along with the 95% confidence interval of the annual sum of carbon exchange, were estimated.

3. Results

3.1 Carbon dioxide flux data characteristics

316   To model the high-quality carbon flux data, the 30-min carbon flux data with high signal
317   quality were screened. It can be seen that the flux observation points exhibit more obvious carbon
318   uptake characteristics during the growing season (Fig. 3). To extract the nighttime flux error, the
319   nighttime friction velocity thresholds for the growing and non-growing seasons were estimated,
320   and the data on friction velocities less than the threshold were screened and eliminated. This
321   amounted to approximately 2.4% of the data (415 data points). After processing for outliers and
322   nighttime friction velocity threshold screening, approximately 35.9% (or 6,293 observations) of
323   the high-quality data remained, which was then used to build and test the model (Table 2). Among
324   these measurements, there were 2,892 valid daytime observations (~16.5%) and 1,032 valid
325   nighttime observations during the growing season (~5.9%). There were 1,583 valid daytime
326   observations (~9%) and 786 (~4.5%) valid nighttime observations during the non-growing season.

327   **Fig. 3.** Mean diurnal courses of high-quality 30-min F_C measurements averaged over 2-month
328   periods after filtering: (a) Jan–Feb, (b) Mar–Apr, (c) May–Jun, (d) Jul–Aug, (e) Sep–Oct, and
329   (f) Nov–Dec.

330   Within the boxes, the horizontal bars indicate medians, while the tops and bottoms of the
331   boxes illustrate the 75th and 25th quartiles, respectively. Small circles represent outliers in the
332   observations.

333   **Fig. 4.** Histogram of the data gap distribution

334   This study defined the length of time in which data were continuously missing as the missing
335   time window. A histogram plot was used to display the distribution of the missing time window
336   (Fig. 4). The average length of the missing time window for the flux data was 5.8 h; a total of 24
337   missing time windows were longer than 24 h, mainly concentrated in the non-growing season; the
338   longest missing time window was 30 days (Fig. 5). It can be seen that wind speed and friction
339   velocity u^* differed significantly between the growing and non-growing seasons (Fig. 6). The
340   details of the relationship between u^* and wind speed using SMA regression are presented in Table
341   3 and Fig. 6c. The slopes of the SMA regression for the growing and non-growing seasons were
342   not equal, indicating that the roughness index varied considerably with season.

343   **Table 2.** Quality control procedures for the 30-min flux data

344   **Fig. 5.** Time of F_C and friction velocity u^* observation times over the study year

345   Red, orange, and gray represent Qc = 0, Qc = 1, and Qc = 2, respectively.

346   The nighttime friction velocity threshold during the growing season was 0.12 m/s, and the
347   corresponding value for the non-growing season was 0.10 m/s. Detailed information concerning
348   the quality filtering procedures is listed in Table 2. A total of 42 negative F_C values were observed
349   at night in this study, accounting for 1.9% of the nighttime data. After removal by the friction
350   velocity threshold and other quality filtering procedures, the number of nighttime negative values
351   was reduced to 16 (~0.7%).

352   **Table 3.** Standardized major axis estimation and statistical inference

353   **Fig. 6.** Values of nighttime friction velocity u^* and wind speed

354   (a) Nighttime friction velocity u^*. (b) Nighttime wind speed. (c)The relationship between
355   friction velocity and wind speed for all data was grouped by season. Green and gray represent
356   the growing and non-growing seasons, respectively. Columns with different capital letters are
357   significantly different ($p < 0.05$) according to Fisher's least significant difference test.

3.2 Results and residual analysis of gap-filling methods

359   The results of the ANN, GP, HLM, RBF, and MDS methods are illustrated in Fig. 7. The test
360   set R^2 obtained by these different methods ranged from 0.77 to 0.84 and the RMSE ranged from
361   2.04 to 2.50 μmol m^{-2} s^{-1}. There were differences in the R^2 and RMSE obtained by these methods.
362   The GP and MDS methods represented the full range of scatter in the observations, while the others
363   all exhibited the upper and lower limits (Fig. 7). The training set fit curve overlapped with the test
364   set fit curve, and they were equally close to the 1:1 line, indicating that there was no overfitting
365   phenomenon in these methods. The gap-filled F_C for the five methods exhibited a relatively
366   obvious diurnal variation (Fig. 8).

367   **Fig. 7.** Training and test performances of the models for the dataset with 6,293 points

368   (a)ANN, (b)GP, (c)HLM, (d)RBF, (e) MDS. For comparison, the plotted lines consist of the
369   training fit (solid black line), the test fit (green dotted line), and the 1:1 line (solid red). Units
370   of RMSE and BE are μmol m^{-2} s^{-1}.

371   **Fig. 8.** Fingerprints of the complete F_C gap-filled by the (a) ANN, (b) GP, (c) HLM, (d) RBF,
372   and (e) MDS methods

373   When model error is quantified, the model residuals can quantify the random uncertainty. In
374   this study, it was assumed that model error was negligible. Thus, the model residuals could be
375   attributed almost entirely to random error. The empirical distribution of the model residuals and
376   the fitted curves (Fig. 9) can describe the uncertainty of the random error and largely reflects the
377   nature of the carbon flux observations. The model residual distributions obtained by the five
378   methods exhibited characteristics of sharp peaks and thick tails, indicating non-normality.
379   Comparing the kurtosis for the empirical distributions of the residuals obtained by these methods
380   (Fig. 9), it was found that GP > MDS > ANN > HLM > RBF. Additionally, the empirical

381 distribution of these residuals was discovered to approximate the Laplace (or double-exponential)
382 distribution by the Wilcoxon rank sum test (p > 0.05).

383 **Fig. 9.** Empirical distributions of the residuals predicted by the five gap-filling methods and
384 their corresponding Laplacian distributions

385 (a)ANN, (b)GP, (c)HLM, (d)RBF, (e)MDS.

386 Comparing the correlations between the carbon flux observations and the corresponding
387 residuals obtained by the 5 different methods (Table 4), it was found that during the day in the
388 non-growing season, $Rd \leq 400$ W m^{-2} showed a significant weak positive correlation; the same
389 was true at night in the non-growing season. Additionally, it was shown that the random
390 uncertainty during the non-growing season increased with increasing carbon flux. The
391 correlations between the flux prediction values and the residuals obtained by the 5 methods
392 differed during the growing season. In the growing season, the GP and MDS methods each
393 exhibited a significant positive correlation, while the other methods showed either a relatively
394 weak correlation (τ close to 0) or no significant correlation.

395 **Table 4.** Kendall's tau (τ) coefficient between the 5 different methods of carbon flux
396 prediction and the corresponding residuals

397 The standard deviation of the random flux measurement error varied linearly with the
398 magnitude of the F_C. Results are summarized in Table 5. The range of the intercept term a of the
399 flux observation station in this study was 1.3209–1.5550 μmol m^{-2} s^{-1}, which is within the typical
400 range. The largest values came from the MDS method; the smallest from the GP. The
401 uncertainties of the carbon flux gap-filling from these 5 methods were ranked as follows: GP <
402 ANN < RBF < HLM < MDS. The slope b ranged from 0.0579–0.1092, which was slightly less
403 than the typical range. The smallest slope came from the HLM; the largest from the MDS. The
404 posterior residual of the carbon flux gap-filling from the HLM method was closer to white noise
405 than that from the MDS method. The carbon flux data gaps were filled by the different methods.
406 The probability distributions of the measured random errors varied with changes in the different
407 gap-filling methods; the gap-filling methods also affected the estimation of the annual sum of
408 carbon dioxide exchange.

409 **Table 5.** Relationship between the magnitude of carbon flux and the standard deviation of
410 random uncertainty

411 *3.3 Annual sum of carbon dioxide exchange*

412 Utilizing the gap-filling from the 5 methods, the complete carbon flux data were obtained. As
413 shown in Table 6, the gap-filled annual F_C sums from MC simulations were estimated to be -
414 159.91 ± 18.35 g C m^{-2} yr^{-1} for ANN, -178.25 ± 8.01 g C m^{-2} yr^{-1} for GP, -167.16 ± 19.08 g C m^{-}
415 ^{2} yr^{-1} for RBF, -156.95 ± 3.15 g C m^{-2} yr^{-1} for HLM, and -155.21 ± 5.16 g C m^{-2} yr^{-1} for MDS. The
416 CO_2 exchange sums from MC simulations for the growing and non-growing seasons are listed in

417   Table 7. Given that five different gap-filling models were used, it was definitely necessary to
418   correct the model error. Based on the chosen fusion method (Kuncheva, 2002), it was assumed
419   that the mean of the 5 methods was close to the true value of the annual sum of carbon dioxide
420   exchange. The annual sum of CO_2 exchange in 2015 at the observed site was estimated to be -
421   163.50 ± 9.43g C m^{-2} yr^{-1}, indicating that the desert Tugai forest in the Ebinur Lake Basin is a net
422   carbon sink on an annual basis.

423   **Table 6.** Annual sum and deviation of the CO_2 exchange estimated by the different methods

424   **Table 7.** Seasonal sum of CO_2 exchange estimated by the different methods

425   The averages of the annual sum of CO_2 exchange obtained by the 5 methods ranged from -
426   178.25 to -155.21 g C m^{-2} yr^{-1}, and the standard deviation ranged from 3.15–19.08 g C m^{-2} yr^{-1}
427   (Table 6). The smallest (in terms of absolute value) came from the MDS method, and the largest
428   from the RBF. The average bias of the annual sum of ecosystem carbon exchange for the 5 methods
429   ranged from -13.69 to 14.05 g C m^{-2} yr^{-1}. The HLM and MDS tended to underestimate, while the
430   other methods tended to overestimate (Table 6). The smallest mean bias of the annual sum of
431   carbon exchange came from the ANN; the largest was from the RBF. The GP had the smallest
432   95% confidence interval for the bias of the annual sum of carbon dioxide exchange, while the
433   HLM had the largest. Comparing the carbon accumulation losses of ecosystems estimated by the
434   different methods (Fig. 10), it was found that these five methods exhibited a consistent
435   performance during the growing season and large differences during the non-growing season.

436   **Fig. 10.** Cumulative carbon dioxide exchange obtained by the different methods

437   The data sources were composed of 3 parts, which were high-quality modeling data, data used
438   to calculate annual sum of carbon dioxide exchange, and predictions from the different gap-
439   filling methods.

440   **4. Discussion**

441   *4.1 Differences in annual sums of CO_2 exchange among gap-filling methods for the Tugai forest*

442   The annual sum of carbon dioxide exchange from the Tugai forest in our study was estimated
443   to range from -178.25 to -155.21 g C m^{-2} yr^{-1}. In a previous study, a total annual carbon exchange
444   ranging from -155 to -55 g C m^{-2} yr^{-1} for oak/grass savanna from 2000–2006 was obtained (Ma et
445   al., 2007), slightly less than the estimated value in this investigation. For comparison, Wohlfahrt
446   et al. (2008) reported a net sink from 102 to 110 g C m^{-2} yr^{-1} in the Mojave desert ecosystem. For
447   a desert shrub community in Baja California/Mexico, the total annual carbon dioxide exchange
448   was determined to range from -52 to -39 g C m^{-2} yr^{-1} (Hastings et al., 2005). In a riparian forest
449   with similar mean annual temperature and precipitation, Ma et al. (2017) reported a net carbon
450   sink from 278 g C m^{-2} yr^{-1} to 427 g C m^{-2} yr^{-1}. Thus, the carbon sink capacity of the Tugai forest
451   in the Ebinur Lake Basin is higher than that of the savanna in the Mojave Desert ecosystem of
452   California and the desert shrub in Baja California/Mexico, while lower than the riparian forest.

453   The performances of the gap-filling methods in this study were comparatively good. It is
454   difficult to determine the best applicability of the gap-filling methods in the desert Tugai forest via
455   a single statistical parameter. Therefore, this study comprehensively evaluated the gap-filling
456   models using R^2, RMSE, and BE. It was found that the test set R^2 obtained by the ANN method
457   was 0.827. The test set R^2 obtained by Menzer et al. (2015) using the ANN method was 0.740,
458   which was 8% lower than this study. The R^2 value obtained by the GP method was 0.844, which
459   was 6% higher than that of Menzer et al. (2015); R^2 obtained by the RBF method was 0.790, which
460   was 39% higher than that of Lärvi et al. (2012) and 3% higher than that of Menzer et al. (2015).
461   The RMSE of the test set obtained by the 5 methods ranged from 2.04–2.50 µmol m^{-2} s^{-1}, which
462   was smaller than that of Lärvi et al. (2012) and Menzer et al. (2015). This may be primarily due to
463   the fact that the estimations by Lärvi et al. (2012) and Menzer et al. (2015) were conducted on
464   urban ecosystems in which the underlying surface of the observation sites was rougher, and the
465   environmental factors affecting carbon dioxide exchange were more complex. Although the eddy
466   covariance method requires that the underlying surface be uniform and flat, the position of the
467   terrain is not absolutely guaranteed in the actual selection process of the underlying surface. In
468   addition, when screening the modeling data, data with a signal quality of 2 were excluded (Järvi
469   et al., 2012). In the current study, however, all data with a signal quality other than 0 (including 1
470   and 2) were excluded, resulting in high modeling data quality. It is clear that the selection of
471   modeling data is particularly important when training models.

472   There were minor differences among the standard deviations of the annual sum of carbon
473   dioxide exchange obtained by the 5 methods. Due to the low annual sum of arid desert ecosystem
474   carbon dioxide exchange, its estimation is sensitive to data processing methods, with some
475   methods possibly leading to bias (Liu et al., 2010). In addition, the soil volume water content data
476   were distorted as a result of the high degree of soil salinization. Therefore, this study ignored the
477   impact of soil moisture on carbon dioxide flux, leading to a very large difference in the annual sum
478   of carbon dioxide exchange obtained by the 5 methods. It should be noted that this study was
479   limited to the seasonal signal from only a single year's worth of data at the site. Future studies
480   should utilize a longer dataset, which would provide more insight into the ecological functioning
481   of the site.

482   The bias error of the annual sum of carbon dioxide exchange obtained by the 5 methods
483   ranged from -13.69 to 14.05 g C m^{-2} yr^{-1}. The minor differences found in the bias error may be
484   related to the fact that the carbon source/sink function of the Tugai forest is more affected by
485   environmental factors than that of other ecosystems, especially soil moisture content. The impact
486   of data processing methods on the estimation of the annual sum of carbon dioxide exchange was
487   discovered to be highly variable, which may be related to the sensitivity of arid desert ecosystems
488   to environmental factors, as well as the definition of valid data.

489   *4.2 Carbon dioxide exchange during nighttime and non-growing season daytime*

490   This study used a quantile-based method to determine the outliers, and also identified and
491   deleted the anomalies in the F_C time series. After careful screening during data preprocessing, a
492   total of 42 negative values of carbon dioxide exchange at night were observed, accounting for

493 1.9% of the nighttime data, which was far less than the 28% of temperate broadleaf forest
494 observations (Thomas et al., 2011). The negative carbon flux observations indicate that there was
495 carbon uptake in the underlying vegetation of the flux tower at night, although this phenomenon
496 was unlikely (Thomas et al., 2011). There is currently no unified view to explain this phenomenon,
497 ignoring atmospheric advection and precipitation as possible causes. Moreover, there is also a
498 systematic error that stems from ignoring the atmospheric advection and precipitation
499 measurements. Even though advection correction is attractive from a theoretical point of view, it
500 is unlikely that air advection characteristics varied over the observed period and sites
501 (Feigenwinter et al., 2008).

502 The accumulation of carbon dioxide exchange obtained by the 5 different methods performed
503 consistently during the growing season and exhibited very large differences during the non-
504 growing season (Fig. 10). During the growing season, the carbon flux data were relatively
505 complete, with no long gaps; the carbon flux data during the non-growing season, however, had
506 more gaps, and the continuously missing time windows were long (Fig. 5), leading to very large
507 differences in method performance. The five methods displayed obvious carbon uptake
508 characteristics in February (Fig. 10), which was consistent with the daily variation characteristics
509 of the selected high-quality modeling data from January and February (Fig. 3a). This result may
510 have been influenced by ignoring the advection and storage terms, which produced a certain
511 systematic error (Bowling et al., 2010). In addition, the high saline alkali water and soil played an
512 important role in the carbon uptake (Li et al., 2015; Ma et al. 2013; Xie et al. 2009).

513 To some extent, the valid data observed at the site depend on independent processes
514 influenced by the geographic environment of the observatory. The resulting uncertainty is
515 primarily random, depending on both the missing time window and the gap-filling method. The
516 friction velocity u^* is intended to capture the turbulent characteristics in the vicinity of the surface.
517 Nighttime data under unsteady conditions are often removed by u^* threshold screening. Each site
518 has a specific u^* threshold that is expected to vary over time (Béziat et al., 2009; Moureaux et al.,
519 2008). The nighttime friction velocity threshold (0.12 m/s) during the growing season was greater
520 than the corresponding value for the non-growing season (0.10 m/s), indicating that the flux
521 observation station experienced different air turbulence characteristics during different seasons
522 (Fig. 6). A possible reason for this is simply that the air temperature during the growing season is
523 higher than during the non-growing season. According to the turbulence intensity theorem, the
524 turbulence intensity is a function of both velocity and temperature shears (Hu et al., 2007). The
525 near-surface temperature changes more rapidly during the growing season night than during the
526 non-growing season night. Thus, in the near-surface layer, the temperature shear formed during
527 the growing season night is larger than that formed during the non-growing season night. In
528 addition, due to vegetation growth, the underlying surface roughness of the observatory is higher
529 during the non-growing season than during the growing season (Fig. 6c). Uncertainty may still
530 exist after u^* threshold screening. There is no guarantee that the data screening process will
531 eliminate all bad data, nor that only bad data will be removed.

532 *4.3 Uncertainty analysis*

533   All measurements have errors or uncertainties (Taylor 1997), and measurement uncertainty
534 includes random and systematic uncertainties (ISO/IEC 2008). Systematic error is considered to
535 be a constant but unknown deviation (Abernethy et al., 1985) and must be estimated by empirical,
536 theoretical, or supplementary measurements. Systematic error cannot be determined by statistical
537 analysis of the measured data itself, nor can it be reduced by averaging. The bootstrapping method
538 has been used to quantify the random uncertainty of the flux integral at different time scales (Wang
539 et al., 2015). In addition, the Monte Carlo method is used to estimate the transmission of
540 uncertainty over longer time scales, particularly the uncertainty associated with gap filling (Moffat
541 et al., 2007).

542   Comparing the change in the empirical distribution of the residuals obtained by the five gap-
543 filling methods (Fig. 9), it was discovered that the empirical distribution of these residuals
544 approximated the Laplace (or double-exponential) distribution. Actually, the distribution of the F_C
545 random error from the Tugai forest ($|F_C| < 10$ μmol m^{-2} s^{-1}) is leptokurtic. As a characteristic of
546 random uncertainty, the leptokurtic distribution has been shown to be robust across a variety of
547 sites and ecosystem types (Hollinger and Richardson, 2005; Richardson et al., 2008; Stauch et al.,
548 2008; Lasslop et al., 2008; Liu et al., 2008; Wang et al., 2015). It has been suggested that the
549 leptokurtic distribution is the result of a superposition of Gaussian distributions and a non-constant
550 variance (Hollinger et al., 2004; Lasslop et al., 2008). After normalizing the error (i.e., dividing
551 each flux observation by the expected standard deviation), its distribution approximated a Gaussian
552 distribution (Richardson et al., 2008).

553   We also found that the random uncertainty increased with increasing carbon flux (Table 5).
554 This was consistent with the findings of Richardson et al. (2008) for the uncertainty of carbon
555 flux measurements from model residuals. Using different methods to fill gaps leads to the
556 differences among the distributions of the measured random errors and affects the estimation of
557 the annual sum of carbon dioxide exchanges. Considering the differences in site characteristics
558 and types of ecosystems, as well as the degree to which the valid flux data are contaminated with
559 data from a separate (nonbiological or atmospheric) process, it is necessary to evaluate random
560 uncertainty carefully and site specifically. This study may provide a valid method for evaluating
561 the gap-filling uncertainty of other types of ecosystems.

562 5. Conclusions

563   This study estimated the annual sum of carbon dioxide exchange of the Tugai forest in the
564 Ebinur Lake Basin of Northwest China in 2015. Selective system errors were corrected by
565 determining the friction velocity threshold and utilizing it to extract high-quality data on the
566 growing and non-growing seasons. Five different methods were used to fill the gaps in the carbon
567 flux time series. These methods all exhibited higher R^2 and lower RMSE values than previous
568 techniques. The GP method was the best of these gap-filling techniques. Uncertainty was inferred
569 from the model residuals; the distribution of the residuals exhibited non-normal properties of
570 spikes and thick tails. The ultimate goal of this investigation was not to select the best gap-filling
571 method by comparing the merits of each but to estimate the uncertainty caused by the gap-filling
572 and to correct model error. The total annual carbon exchange of the Tugai forest at the observation

573 site in 2015 was -163.50 ± 9.43 g C m^{-2} yr^{-1}, indicating that the Tugai forest in the Ebinur Lake
574 Basin is a carbon sink. The errors from different sources were complex, making it difficult to give
575 accurate estimates; therefore, this study only estimated the random errors and bias. Estimating
576 errors from different sources will be the focus of uncertainty studies on the cumulants of carbon
577 dioxide exchange in the future. Exploring the function of the Tugai forest in arid regions still
578 requires additional understanding of the underlying ecological mechanisms.

579 **Acknowledgments:** This research was supported by the National Natural Science Foundation of
580 China (No. 31560131). We thank LetPub (www.letpub.com) for its linguistic assistance during the
581 preparation of this manuscript.

582 **References**

583 Abernethy R, Benedict R, and Dowdell R. 1985. ASME measurement uncertainty. *Journal of Fluids Engineering*
584   107:161.
585 Aubinet M, and Feigenwinter C. 2010. Direct CO_2 advection measurements and the night flux problem. *Agricultural*
586   *and Forest Meteorology* 150:651-654. 10.1016/j.agrformet.2010.03.007
587 Azmy WM, El Gayar N, Atiya AF, and El-Shishiny H. 2009. MLP, Gaussian Processes and Negative Correlation
588   Learning for Time Series Prediction. *Multiple Classifier Systems, Proceedings* 5519:428-+.
589 Baldocchi D. 2014. Measuring fluxes of trace gases and energy between ecosystems and the atmosphere - the state
590   and future of the eddy covariance method. *Global Change Biology* 20:3600-3609. 10.1111/gcb.12649
591 Baldocchi D, Chu HS, and Reichstein M. 2018. Inter-annual variability of net and gross ecosystem carbon fluxes:
592   A review. *Agricultural and Forest Meteorology* 249:520-533. 10.1016/j.agrformet.2017.05.015Béziat
593   P, Ceschia E, and Dedieu G. 2009. Carbon balance of a three crop succession over two cropland sites in
594   South West France. *Agricultural and Forest Meteorology* 149:1628-1645.
595 Bishop CM. 2006. *Pattern Recognition and Machine Learning (Information Science and Statistics)*.
596 Bowling DR, Bethers-Marchetti S, Lunch CK, Grote EE, and Belnap J. 2010. Carbon, water, and energy fluxes in a
597   semiarid cold desert grassland during and following multiyear drought. *Journal of Geophysical Research*
598   115. 10.1029/2010jg001322
599 Braswell BH, Sacks WJ, Linder E, and Schimel DS. 2005. Estimating diurnal to annual ecosystem parameters by
600   synthesis of a carbon flux model with eddy covariance net ecosystem exchange observations. *Global Change*
601   *Biology* 11:335-355. 10.1111/j.1365-2486.2005.00897.x
602 Desai AR, Bolstad PV, Cook BD, Davis KJ, and Carey EV. 2005. Comparing net ecosystem exchange of carbon
603   dioxide between an old-growth and mature forest in the upper Midwest, USA. *Agricultural and Forest*
604   *Meteorology* 128:33-55. 10.1016/j.agrformet.2004.09.005
605 Donohue RJ, Roderick ML, McVicar TR, and Farquhar GD. 2013. Impact of CO_2 fertilization on maximum foliage
606   cover across the globe's warm, arid environments. *Geophysical Research Letters* 40:3031-3035.
607   10.1002/grl.50563
608 Fahrmeir L, Kneib T, and Konrath S. 2009. Bayesian regularisation in structured additive regression: a unifying
609   perspective on shrinkage, smoothing and predictor selection. *Statistics and Computing* 20:203-219.
610   10.1007/s11222-009-9158-3
611 Falge E, Baldocchi D, Olson R, Anthoni P, Aubinet M, Bernhofer C, Burba G, Ceulemans R, Clement R, Dolman H,
612   Granier A, Gross P, Grunwald T, Hollinger D, Jensen NO, Katul G, Keronen P, Kowalski A, Lai CT, Law

613   BE, Meyers T, Moncrieff H, Moors E, Munger JW, Pilegaard K, Rannik U, Rebmann C, Suyker A, Tenhunen
614   J, Tu K, Verma S, Vesala T, Wilson K, and Wofsy S. 2001. Gap filling strategies for defensible annual sums
615   of net ecosystem exchange. *Agricultural and Forest Meteorology* 107:43-69. Doi 10.1016/S0168-
616   1923(00)00225-2

617 Feigenwinter C, Bernhofer C, Eichelmann U, Heinesch B, Hertel M, Janous D, Kolle O, Lagergren F, Lindroth A,
618   Minerbi S, Moderow U, Mölder M, Montagnani L, Queck R, Rebmann C, Vestin P, Yernaux M, Zeri M,
619   Ziegler W, and Aubinet M. 2008. Comparison of horizontal and vertical advective CO_2 fluxes at three forest
620   sites. *Agricultural and Forest Meteorology* 148:12-24. 10.1016/j.agrformet.2007.08.013

621 Foken T, and Wichura B. 1996. Tools for quality assessment of surface-based flux measurements. *Agricultural &*
622   *Forest Meteorology* 78:83-105.

623 Gelman, and Andrew. 2006. Multilevel (Hierarchical) Modeling: What It Can and Cannot Do. *Technometrics* 48:432-
624   435.

625 Gove JH, and Hollinger DY. 2006. Application of a dual unscented Kalman filter for simultaneous state and parameter
626   estimation in problems of surface-atmosphere exchange. *Journal of Geophysical Research* 111.
627   10.1029/2005jd006021

628 Hagen SC, Braswell BH, Linder E, Frolking S, Richardson AD, and Hollinger DY. 2006. Statistical uncertainty of
629   eddy flux–based estimates of gross ecosystem carbon exchange at Howland Forest, Maine. *Journal of*
630   *Geophysical Research.*

631 Hastings SJ, Oechel WC, and Muhlia-Melo A. 2005. Diurnal, seasonal and annual variation in the net ecosystem CO_2
632   exchange of a desert shrub community (Sarcocaulescent) in Baja California, Mexico. *Global Change Biology*
633   11:927-939. 10.1111/j.1365-2486.2005.00951.x

634 He X, Lv G, and Qin L. 2014. Research on data characteristics during non-growing season of desert-wetland
635   ecosystem in Ebinur Lake. *Acta Ecologica Sinica* 34:6655-6665.

636 He X, Lv G, Qin L, Chang S, Yang M, Yang J, and Yang X. 2015. Effects of Simulated Nitrogen Deposition on Soil
637   Respiration in a Populus euphratica Community in the Ebinur Lake Area, a Desert Ecosystem of
638   Northwestern China. *Plos One* 10:e0137827.

639 Hollinger DY, Aber J, Dail B, Davidson EA, Goltz SM, Hughes H, Leclerc MY, Lee JT, Richardson AD, Rodrigues
640   C, Scott NA, Achuatavarier D, and Walsh J. 2004. Spatial and temporal variability in forest-atmosphere CO_2
641   exchange. *Global Change Biology* 10:1689-1706. 10.1111/j.1365-2486.2004.00847.x

642 Hollinger DY, and Richardson AD. 2005. Uncertainty in eddy covariance measurements and its application to
643   physiological models. *Tree Physiology* 25:873-885. DOI 10.1093/treephys/25.7.873

644 Hu Y, Chen J, and Zuo H. 2007. Theorem of turbulent intensity and macroscopic mechanism of the turbulence
645   development. *Science in China Series D: Earth Sciences* 50:789-800.

646 Hu Y, Chen J, and Zuo H. 2007. Theorem of turbulent intensity and macroscopic mechanism of the turbulence
647   development. *Science in China Series D: Earth Sciences* 50:789-800.

648 Järvi L, Nordbo A, Junninen H, Riikonen A, Moilanen J, Nikinmaa E, and Vesala T. 2012. Seasonal and annual
649   variation of carbon dioxide surface fluxes in Helsinki, Finland, in 2006–2010. *Atmospheric Chemistry and*
650   *Physics Discussions* 12:8355-8396. 10.5194/acpd-12-8355-2012

651 Jasoni RL, Smith SD, and III JAA. 2005. Net ecosystem CO_2 exchange in Mojave Desert shrublands during the eighth
652   year of exposure to elevated CO_2. *Global Change Biology* 11:749–756.

653 Jin H, Bai X, Man Z, and Zan M. 2010. Space difference of soil in Xinjiang Ebinur Lake Wetland Natural Reserve

654   District. *Journal of Arid Land Resources and Environment* 2:150-157.

655   Kormann R, and Meixner FX. 2001. An analytical footprint model for non-neutral stratification. *Boundary-Layer*

656   *Meteorology* 99:207-224. Doi 10.1023/A:1018991015119

657   Kuncheva LI. 2002. A theoretical study on six classifier fusion strategies. *IEEE Transactions on pattern analysis and*

658   *machine intelligence* 24:281-286.

659   Kunwor S, Starr G, Loescher HW, and Staudhammer CL. 2017. Preserving the variance in imputed eddy-covariance

660   measurements: Alternative methods for defensible gap filling. *Agricultural and Forest Meteorology* 232:635-

661   649. 10.1016/j.agrformet.2016.10.018

662   Lasslop G, Reichstein M, Kattge J, and Papale D. 2008. Influences of observation errors in eddy flux data on inverse

663   model parameter estimation. *Biogeosciences Discussions* 5:751-785.

664   Li S, Asanuma J, Eugster W, Kotani A, Liu J, Urano T, Oikawa T, Davaa G, Oyunbaatar D, and Sugita M. 2005. Net

665   ecosystem carbon dioxide exchange over grazed steppe in central Mongolia. *Global Change Biology*

666   11:1941-1955.

667   Li Y, Wang Y-G, Houghton RA, and Tang L-S. 2015. Hidden carbon sink beneath desert. *Geophysical Research*

668   *Letters* 42:5880-5887. 10.1002/2015gl064222

669   Lima CHR, and Lall U. 2010. Spatial scaling in a changing climate: A hierarchical bayesian model for non-stationary

670   multi-site annual maximum and monthly streamflow. *Journal of Hydrology* 383:307-318.

671   Lima CHR, Lall U, Troy T, and Devineni N. 2016. A hierarchical Bayesian GEV model for improving local and

672   regional flood quantile estimates. *Journal of Hydrology* 541:816-823.

673   Liu M, He H, Yu G, Luo Y, Sun X, and Wang H. 2008. Uncertainty analysis of CO_2 flux components in subtropical

674   evergreen coniferous plantation. *Science in China Series D: Earth Sciences* 52:257-268. 10.1007/s11430-

675   009-0010-6

676   Liu M, He H, Yu G, Sun X, Zhu X, Zhang L, Zhao X, Wang H, Shi P, and Han S. 2010. Impacts of uncertainty in

677   data processing on estimation of CO_2 flux components. *Chinese Journal of Applied Ecology* 21:2389-2396.

678   Ma J, Wang ZY, Stevenson BA, Zheng XJ, and Li Y. 2013. An inorganic CO_2 diffusion and dissolution process

679   explains negative CO_2 fluxes in saline/alkaline soils. *Scientific Reports* 3:2025. 10.1038/srep02025

680   Ma J, Liu R, Tang L-S, Lan Z-D, and Li Y. 2014. A downward CO_2 flux seems to have nowhere to go. *Biogeosciences*

681   *Discussions* 11:6251-6262.

682   Ma S, Baldocchi DD, Xu L, and Hehn T. 2007. Inter-annual variability in carbon dioxide exchange of an oak/grass

683   savanna and open grassland in California. *Agricultural & Forest Meteorology* 147:157-171.

684   Ma X, Feng Q, Yu T, Su Y, and Deo R. 2017. Carbon Dioxide Fluxes and Their Environmental Controls in a Riparian

685   Forest within the Hyper-Arid Region of Northwest China. *Forests* 8. 10.3390/f8100379

686   Massman W J, Lee X, Eddy Covariance Flux Corrections and Uncertainties in Long Term Studies of Carbon and

687   Energy Exchanges. *Agricultural and Forest Meteorology* 113:121-144.

688   Mauder M, Cuntz M, Drüe C, Graf A, Rebmann C, Schmid HP, Schmidt M, and Steinbrecher R. 2013. A strategy for

689   quality and uncertainty assessment of long-term eddy-covariance measurements. *Agricultural & Forest*

690   *Meteorology* 169:122-135.

691   Menzer O, Meiring W, Kyriakidis PC, and McFadden JP. 2015. Annual sums of carbon dioxide exchange over a

692   heterogeneous urban landscape through machine learning based gap-filling. *Atmospheric Environment*

693   101:312-327. 10.1016/j.atmosenv.2014.11.006

694   Menzer O, Moffat AM, Meiring W, Lasslop G, Schukat-Talamazzini EG, and Reichstein M. 2013. Random errors in

695   carbon and water vapor fluxes assessed with Gaussian Processes. *Agricultural and Forest Meteorology*
696   178:161-172. 10.1016/j.agrformet.2013.04.024

697 Moffat AM, Papale D, Reichstein M, Hollinger DY, Richardson AD, Barr AG, Beckstein C, Braswell BH, Churkina
698   G, Desai AR, Falge E, Gove JH, Heimann M, Hui D, Jarvis AJ, Kattge J, Noormets A, and Stauch VJ. 2007.
699   Comprehensive comparison of gap-filling techniques for eddy covariance net carbon fluxes. *Agricultural and*
700   *Forest Meteorology* 147:209-232. 10.1016/j.agrformet.2007.08.011

701 Moureaux C, Debacq A, Hoyaux J, Suleau M, Tourneur D, Vancutsem F, Bodson B, and Aubinet M. 2008. Carbon
702   balance assessment of a Belgian winter wheat crop (Triticum aestivum L.). *Global Change Biology* 14:1353-
703   1366.

704 Munir TM, Perkins M, Kaing E, and Strack M. 2015. Carbon dioxide flux and net primary production of a boreal treed
705   bog: Responses to warming and water-table-lowering simulations of climate change. *Biogeosciences* 12:1-
706   21.

707 Ogle K, and Barber JJ. 2008. Bayesian Data—Model Integration in Plant Physiological and Ecosystem Ecology.
708   *Progress in Botany* 69:281-311.

709 Papale D, Reichstein M, Aubinet M, Canfora E, Bernhofer C, Kutsch W, Longdoz B, Rambal S, Valentini R, Vesala
710   T, and Yakir D. 2006. Towards a standardized processing of Net Ecosystem Exchange measured with eddy
711   covariance technique: algorithms and uncertainty estimation. *Biogeosciences* 3:571-583. DOI 10.5194/bg-3-
712   571-2006

713 Papale D, and Valentini R. 2003. A new assessment of European forests carbon exchanges by eddy fluxes and artificial
714   neural network spatialization. *Global Change Biology* 9:525-535. DOI 10.1046/j.1365-2486.2003.00609.x

715 Poulter B, Frank D, Ciais P, Myneni RB, Andela N, Bi J, Broquet G, Canadell JG, Chevallier F, and Liu YY. 2014.
716   Contribution of semi-arid ecosystems to interannual variability of the global carbon cycle. *Nature* 509:600.

717 Rebane S, Jõgiste K, Põldveer E, Stanturf JA, and Metslaid M. 2019. Direct measurements of carbon exchange at
718   forest disturbance sites: a review of results with the eddy covariance method. *Scandinavian Journal of Forest*
719   *Research*:1-13. 10.1080/02827581.2019.1659849

720 Reichstein M, Falge E, Baldocchi D, Papale D, Aubinet M, Berbigier P, Bernhofer C, Buchmann N, Gilmanov T,
721   Granier A, Grünwald T, Havránková K, Ilvesniemi H, Janous D, Knohl A, Laurila T, Lohila A, Loustau D,
722   Matteucci G, Meyers T, Miglietta F, Ourcival J-M, Pumpanen J, Rambal S, Rotenberg E, Sanz M, Tenhunen
723   J, Seufert G, Vaccari F, Vesala T, Yakir D, and Valentini R. 2005. On the separation of net ecosystem
724   exchange into assimilation and ecosystem respiration: review and improved algorithm. *Global Change*
725   *Biology* 11:1424-1439. 10.1111/j.1365-2486.2005.001002.x

726 Richardson AD, Hollinger DY, Burba GG, Davis KJ, Flanagan LB, Katul GG, William Munger J, Ricciuto DM, Stoy
727   PC, Suyker AE, Verma SB, and Wofsy SC. 2006. A multi-site analysis of random error in tower-based
728   measurements of carbon and energy fluxes. *Agricultural and Forest Meteorology* 136:1-18.
729   10.1016/j.agrformet.2006.01.007

730 Richardson AD, Mahecha MD, Falge E, Kattge J, Moffat AM, Papale D, Reichstein M, Stauch VJ, Braswell BH,
731   Churkina G, Kruijt B, and Hollinger DY. 2008. Statistical properties of random CO_2 flux measurement
732   uncertainty inferred from model residuals. *Agricultural and Forest Meteorology* 148:38-50.
733   10.1016/j.agrformet.2007.09.001

734 Ruppert J, Mauder M, Thomas C, and Lüers J. 2006. Innovative gap-filling strategy for annual sums of CO_2 net
735   ecosystem exchange. *Agricultural and Forest Meteorology* 138:5-18. 10.1016/j.agrformet.2006.03.003

736 Schmidt A, Wrzesinsky T, and Klemm O. 2007. Gap Filling and Quality Assessment of CO_2 and Water Vapour Fluxes
737   above an Urban Area with Radial Basis Function Neural Networks. *Boundary-Layer Meteorology* 126:389-
738   413. 10.1007/s10546-007-9249-7

739 Soloway AD, Amiro BD, Dunn AL, and Wofsy SC. 2017. Carbon neutral or a sink? Uncertainty caused by gap-filling
740   long-term flux measurements for an old-growth boreal black spruce forest. *Agricultural and Forest*
741   *Meteorology* 233:110-121. 10.1016/j.agrformet.2016.11.005

742 Stauch VJ, Jarvis AJ, and Schulz K. 2008. Estimation of net carbon exchange using eddy covariance CO_2 flux
743   observations and a stochastic model. *Journal of Geophysical Research* 113. 10.1029/2007jd008603

744 Stone R. 2008. Have Desert Researchers Discovered a Hidden Loop in the Carbon Cycle? *Science* 320:1409-1410.
745   Taylor J. 1997. *Introduction to error analysis, the study of uncertainties in physical measurements*.

746 Thomas MV, Malhi Y, Fenn KM, Fisher JB, Morecroft MD, Lloyd CR, Taylor ME, and McNeil DD. 2011. Carbon
747   dioxide fluxes over an ancient broadleaved deciduous woodland in southern England. *Biogeosciences*
748   8:1595-1613.

749 Wang H, Cai Y, Yang Q, Gong Y, Lv G, 2019. Factors that alter the relative importance of abiotic and biotic drivers
750   on the fertile island in a desert-oasis ecotone. *Science of The Total Environment* 697,
751   doi.org/10.1016/j.scitotenv.2019.134096

752 Wang HJ, Riley WJ, and Collins WD. 2015. Statistical uncertainty of eddy covariance CO_2 fluxes inferred using a
753   residual   bootstrap   approach.   *Agricultural   and   Forest   Meteorology*   206:163-171.
754   10.1016/j.agrformet.2015.03.011

755 Wang J, Ding J, Li G, Liang J, Yu D, Aishan T, Zhang F, Yang J, Abulimiti A, and Liu J. 2019a. Dynamic detection
756   of water surface area of Ebinur Lake using multi-source satellite data (Landsat and Sentinel-1A) and its
757   responses to changing environment. *Catena* 177:189-201.

758 Wang J, Ding J, Yu D, Ma X, Zhang Z, Ge X, Teng D, Li X, Liang J, and Lizaga I. 2019b. Capability of Sentinel-2
759   MSI data for monitoring and mapping of soil salinity in dry and wet seasons in the Ebinur Lake region,
760   Xinjiang, China. *Geoderma* 353:172-187.

761 Warton DI, Duursma RA, Falster DS, and Taskinen S. 2012. smatr 3- an R package for estimation and inference
762   about   allometric   lines.   *Methods   in   Ecology   and   Evolution*   3:257-259.   10.1111/j.2041-
763   210X.2011.00153.x

764 Webb EK, Pearman GI, and Leuning R. 2010. Correction of flux measurements for density effects due to heat and
765   water vapour transfer. *Quarterly Journal of the Royal Meteorological Society* 106:85-100.

766 Williams M, Richardson AD, Reichstein M, Stoy PC, Peylin P, Verbeeck H, Carvalhais N, Jung M, Hollinger DY,
767   and Kattge J. 2009. Improving land surface models with FLUXNET data. *Biogeosciences* 6:1341-1359.

768 Wohlfahrt G, Fenstermaker LF, and Arnone III JA. 2008. Large annual net ecosystem CO_2 uptake of a Mojave Desert
769   ecosystem. *Global Change Biology* 14:1475-1487.

770 Xie J, Li Y, Zhai C, Li C, and Lan Z. 2009. CO_2 absorption by alkaline soils and its implication to the global carbon
771   cycle. *Environmental Geology* 56:953-961.

Figure 1

Aerial photograph of the tower site.

(a) Location map of the Ebinur Lake Basin, (b) Location map of the measurement tower, (c) aerial photo of the tower site in August (Photograph credit: Jinlong Wang), (d) photograph of the tower site in May (Photograph credit: Dexiong Teng), and (e) remote sensing image in June and the average footprint for the entire observation period (Kormann and Meixner, 2001). The measurement tower is marked with a red circle. The white lines represent isopleths of the average contributions.
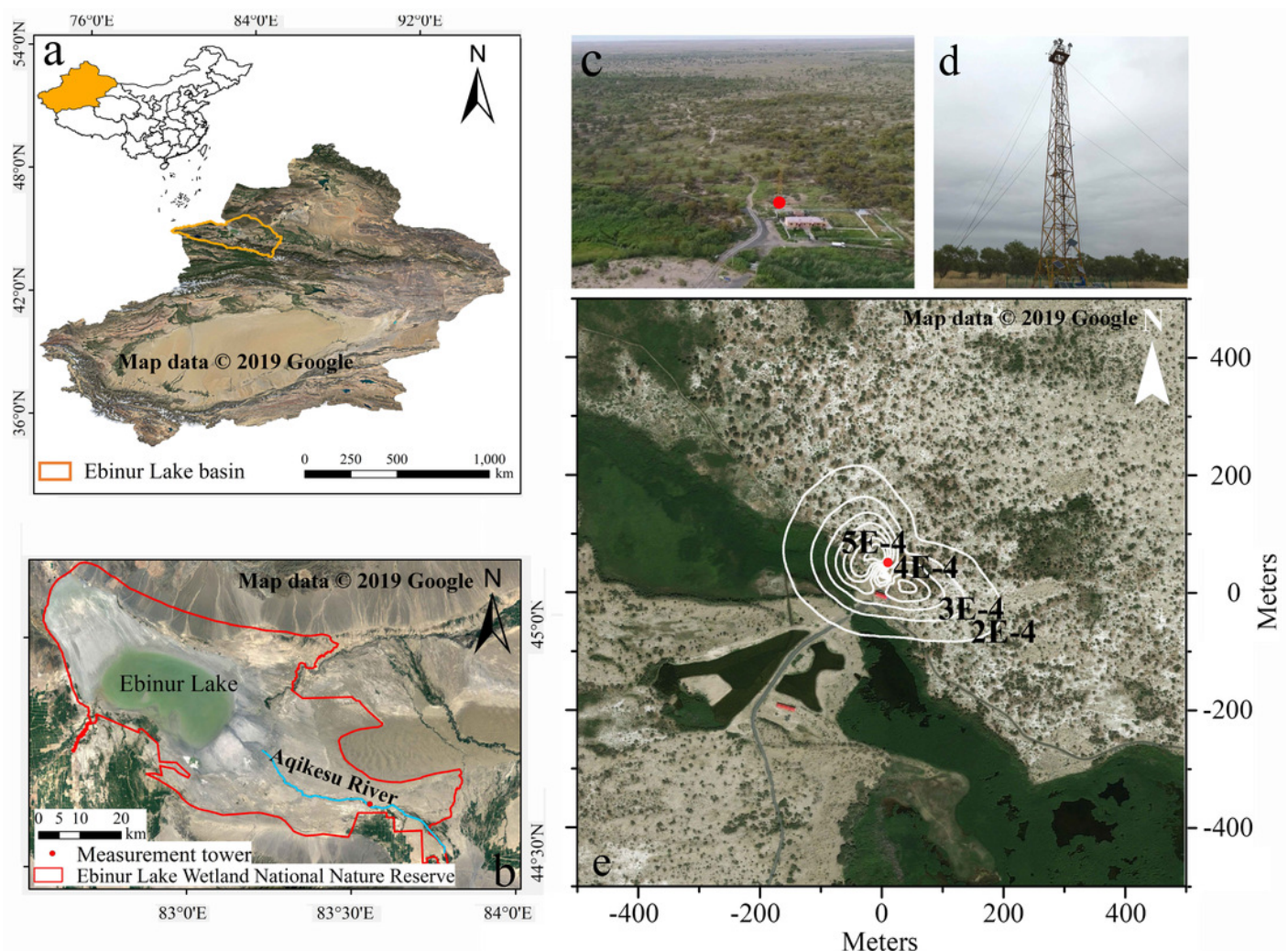
Figure 2

Meteorological observations during the year of measurement

Half-hour averaged values of (a) air temperature (T_{air}), (b) precipitation, (c) global radiation (Rg), (d) wind speed, and (e) relative humidity (RH) during the observation period
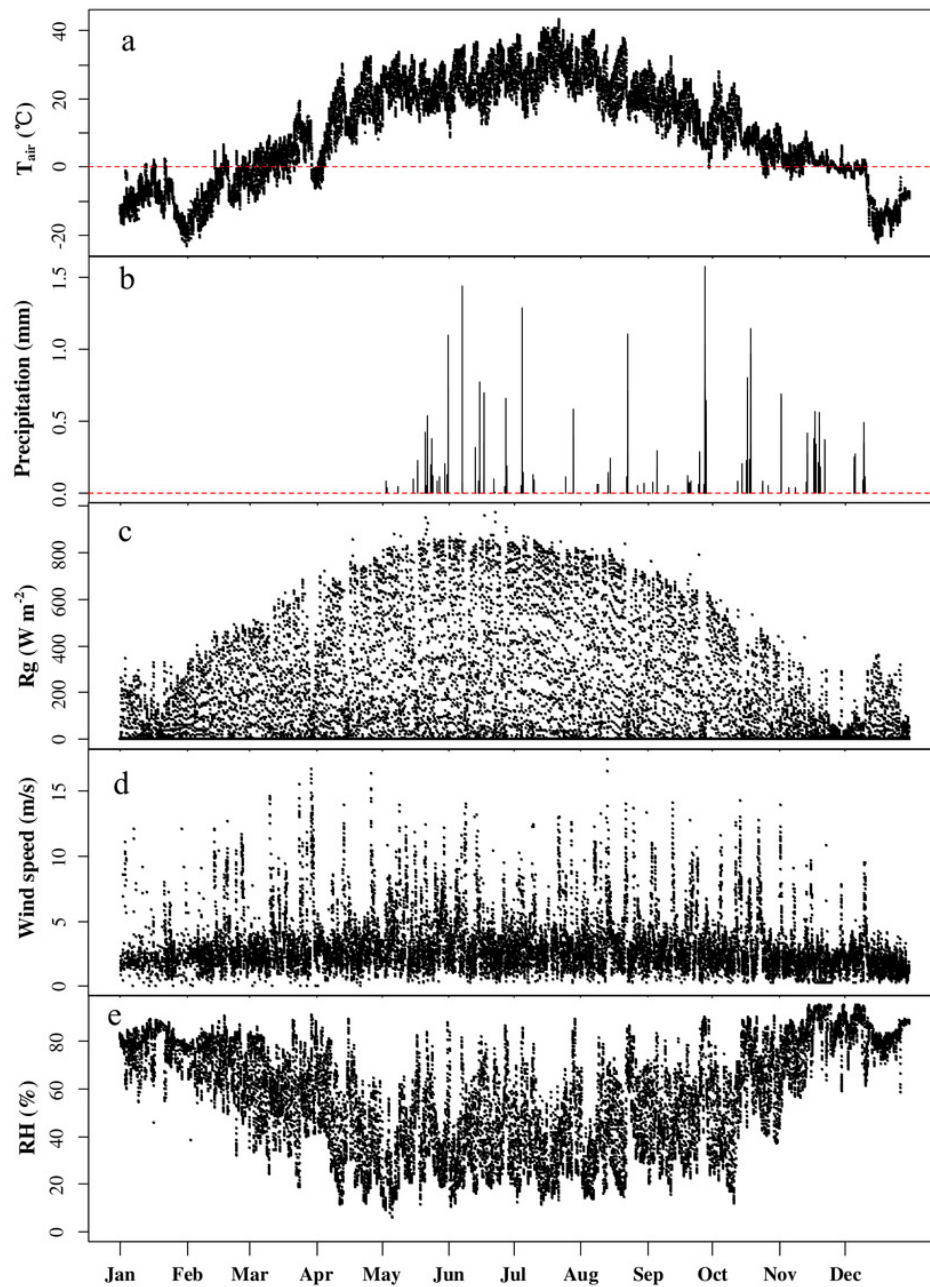
Figure 3

Mean diurnal courses of high-quality 30-min F_C measurements averaged over 2-month periods after filtering: (a) Jan–Feb, (b) Mar–Apr, (c) May–Jun, (d) Jul–Aug, (e) Sep–Oct, and (f) Nov–Dec.

Within the boxes, the horizontal bars indicate medians, while the tops and bottoms of the boxes illustrate the 75th and 25th quartiles, respectively. Small circles represent outliers in the observations.
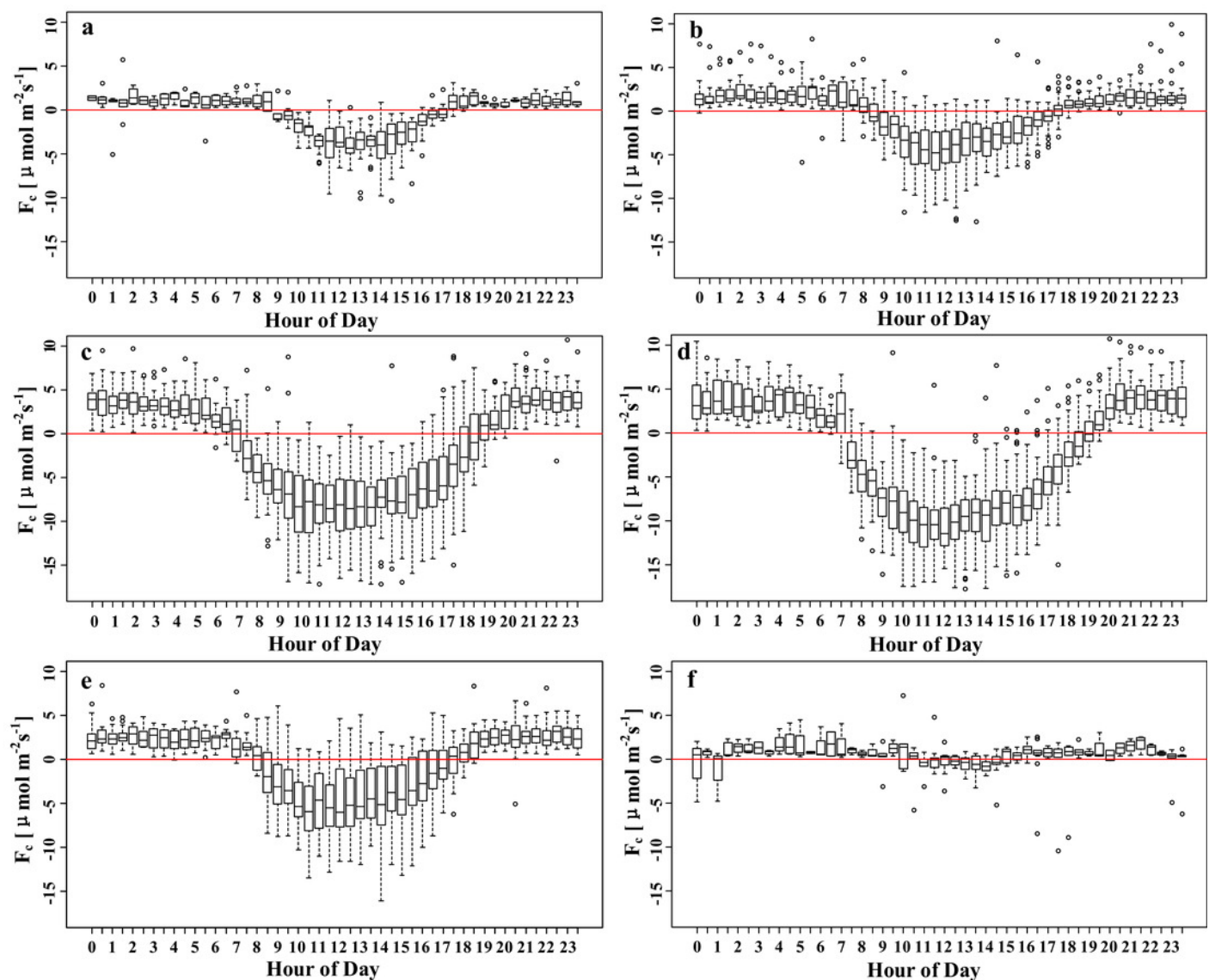
Figure 4

Histogram of the data gap distribution
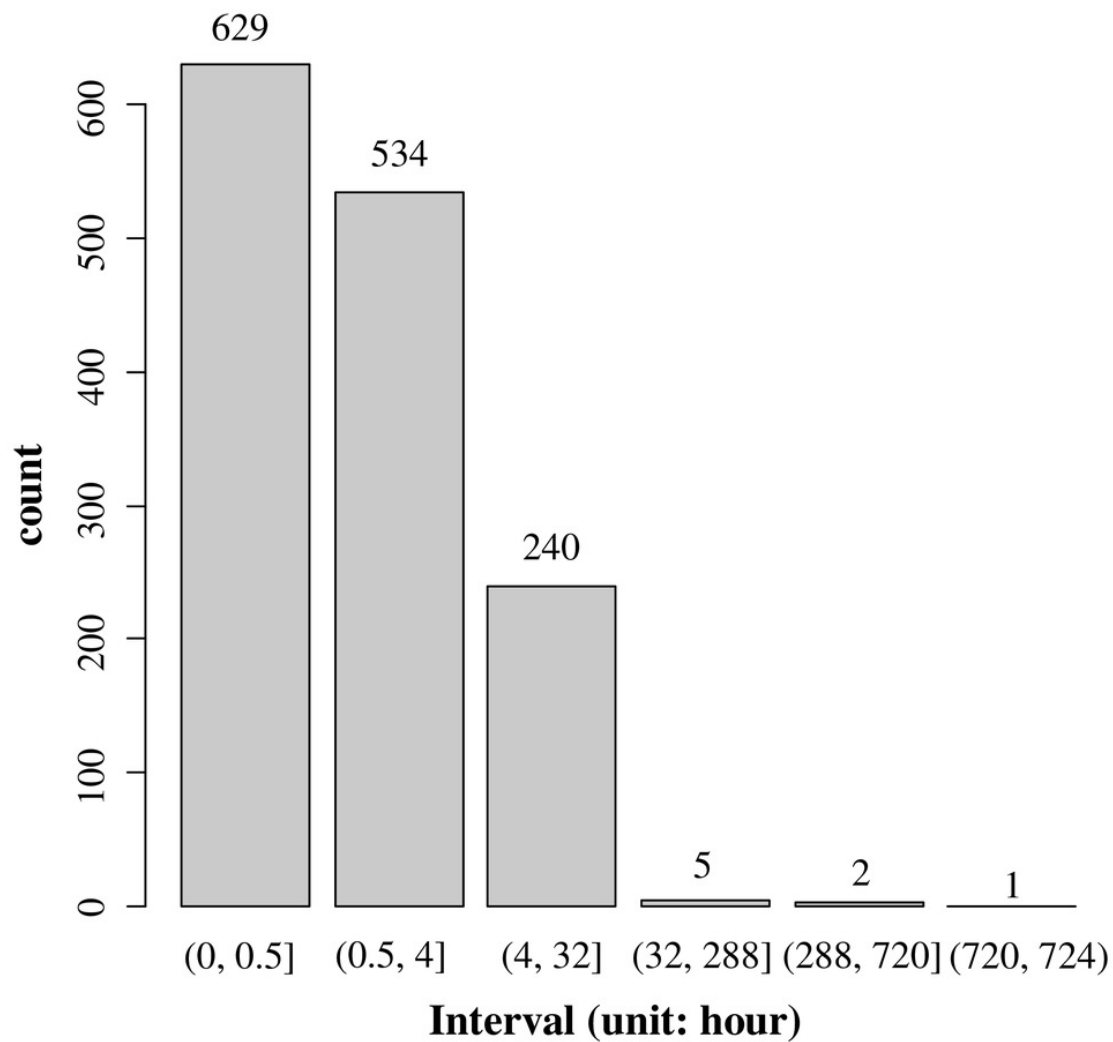
Figure 5

Time of F_C and friction velocity u^* observation times over the study year

Red, green, and blue represent Qc = 0, Qc = 1, and Qc = 2, respectively.
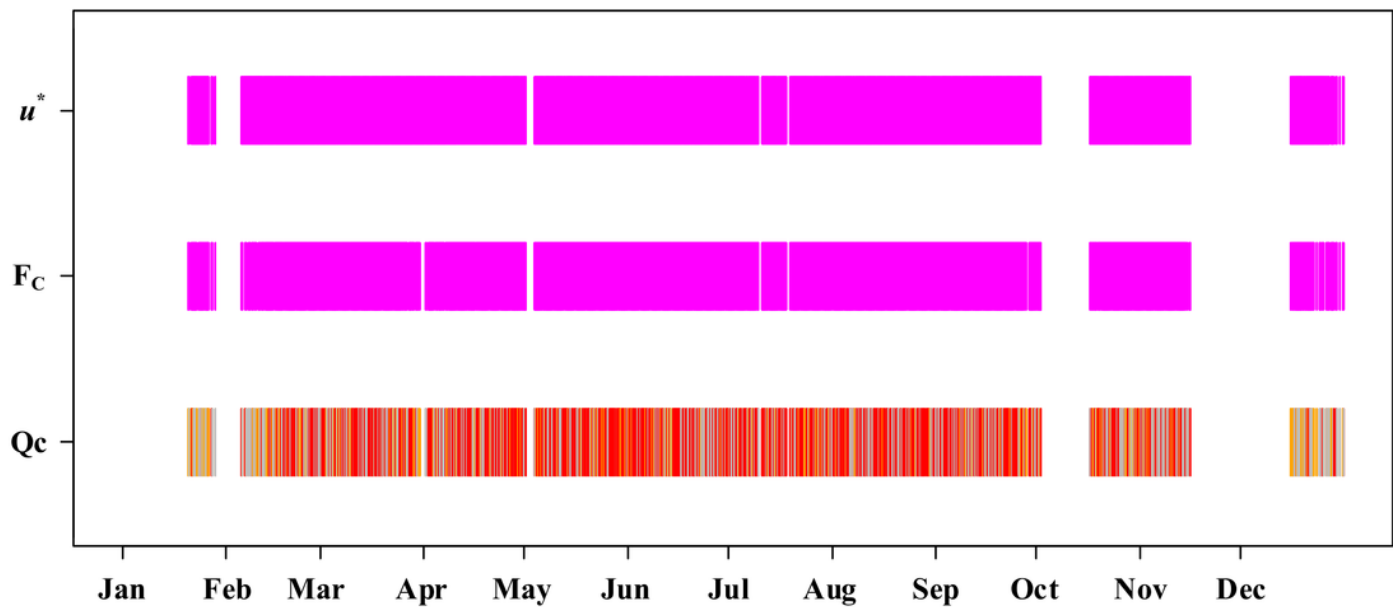
Figure 6

Values of nighttime friction velocity u^* and wind speed

(a) Nighttime friction velocity u^*. (b) Nighttime wind speed. (c)The relationship between friction velocity and wind speed for all data was grouped by season. Green and gray represent the growing and non-growing seasons, respectively. Columns with different capital letters are significantly different ($p < 0.05$) according to Fisher's least significant difference test.
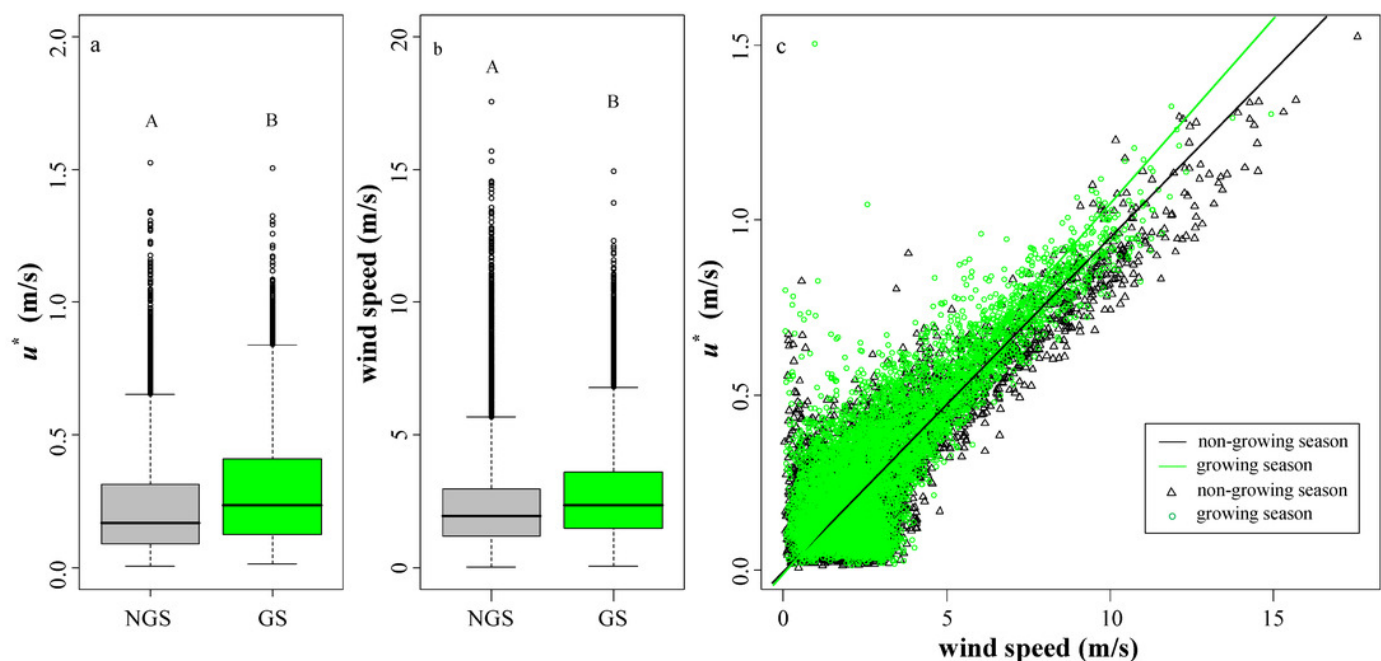
Figure 7

Training and test performances of the models for the dataset with 6,293 points

(a)ANN, (b)GP, (c)HLM, (d)RBF, (e) MDS. For comparison, the plotted lines consist of the training fit (solid black line), the test fit (green dotted line), and the 1:1 line (solid red). Units of RMSE and BE are μmol m^{-2} s^{-1}.
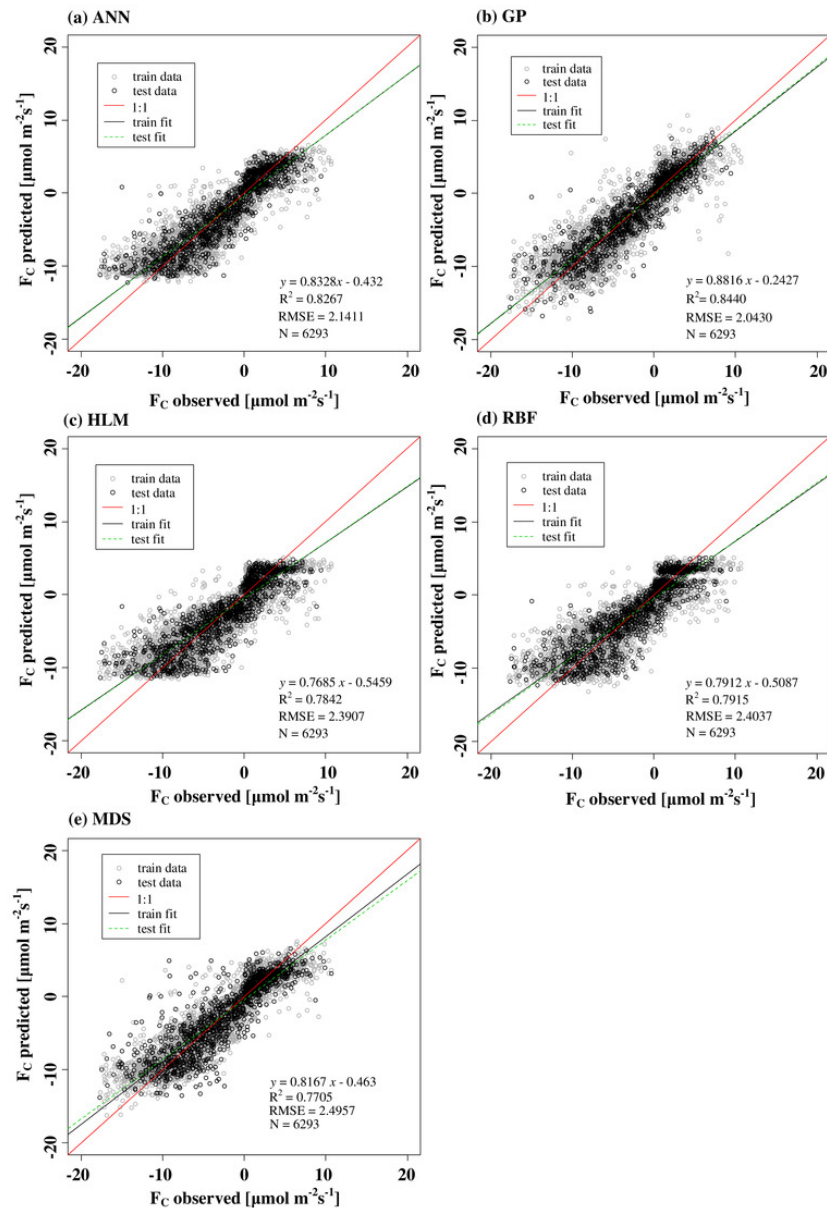
Figure 8

Fingerprints of the complete F_C gap-filled by the (a) ANN, (b) GP, (c) HLM, (d) RBF, and (e) MDS methods
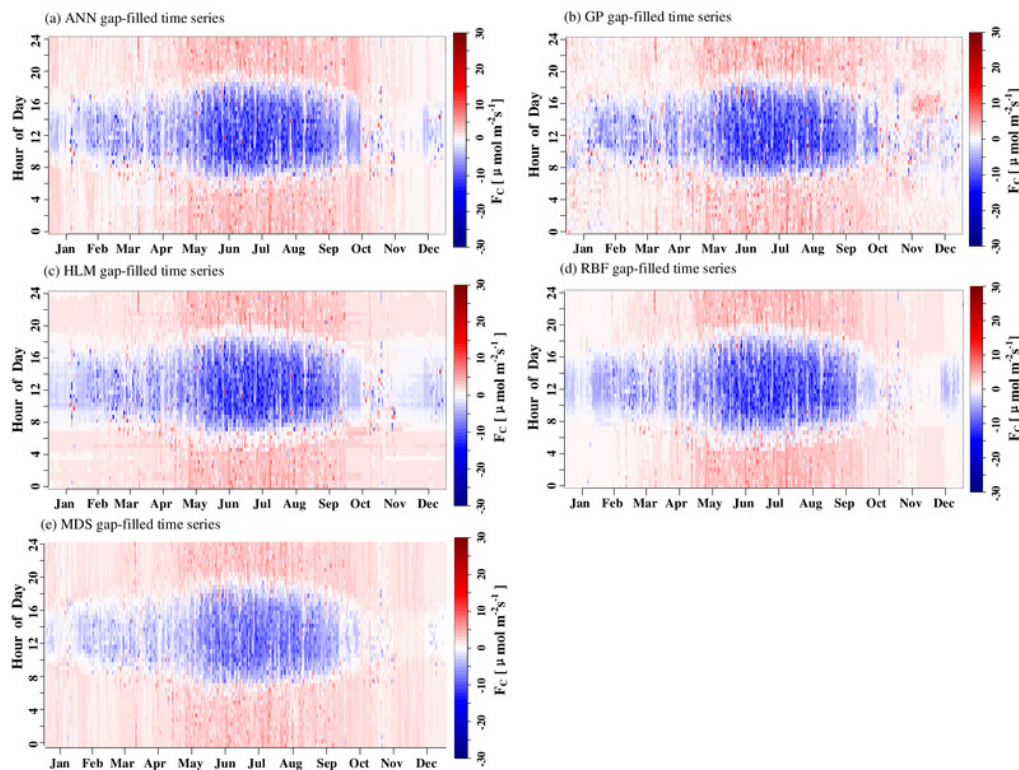
Figure 9

Empirical distributions of the residuals predicted by the five gap-filling methods and their corresponding Laplacian distributions

(a)ANN, (b)GP, (c)HLM, (d)RBF, (e) MDS.
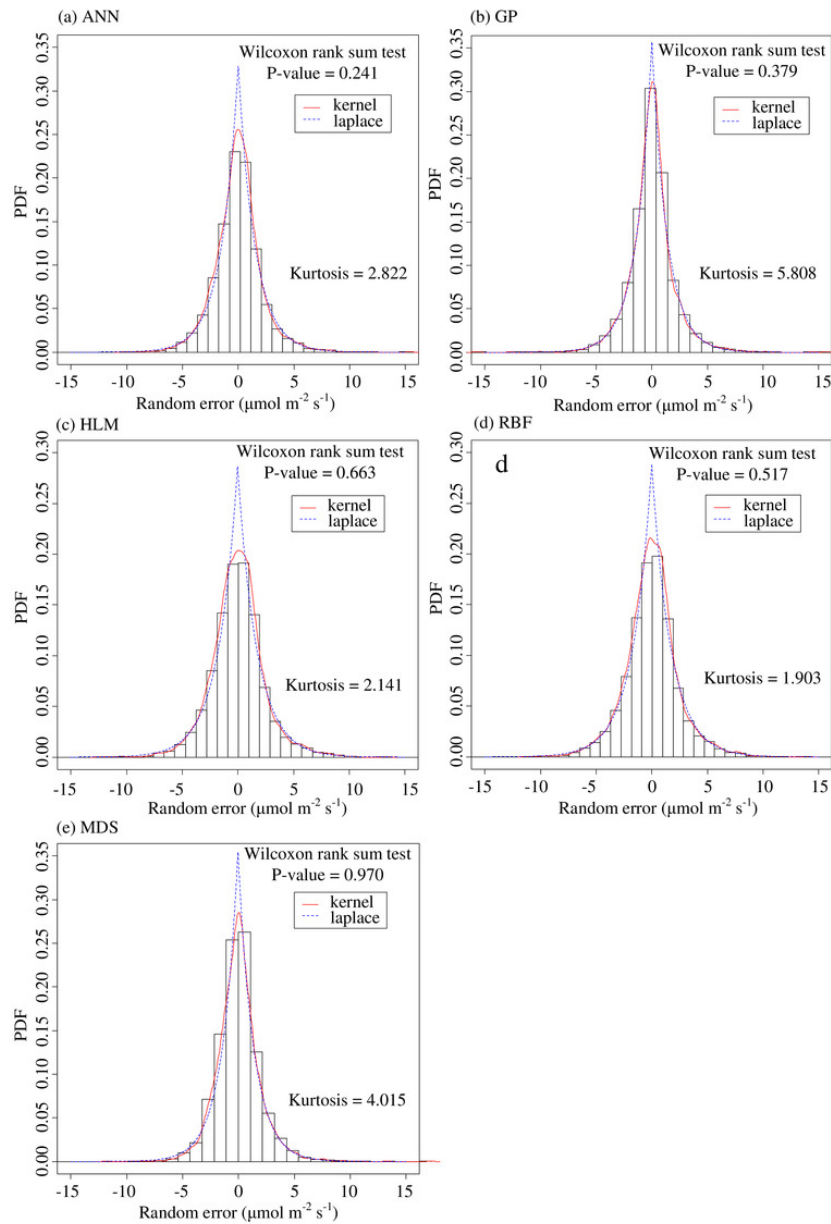
Figure 10

Cumulative carbon dioxide exchange obtained by the different methods

The data sources were composed of 3 parts, which were high-quality modeling data, data used to calculate annual sum of carbon dioxide exchange, and predictions from the different gap-filling methods.
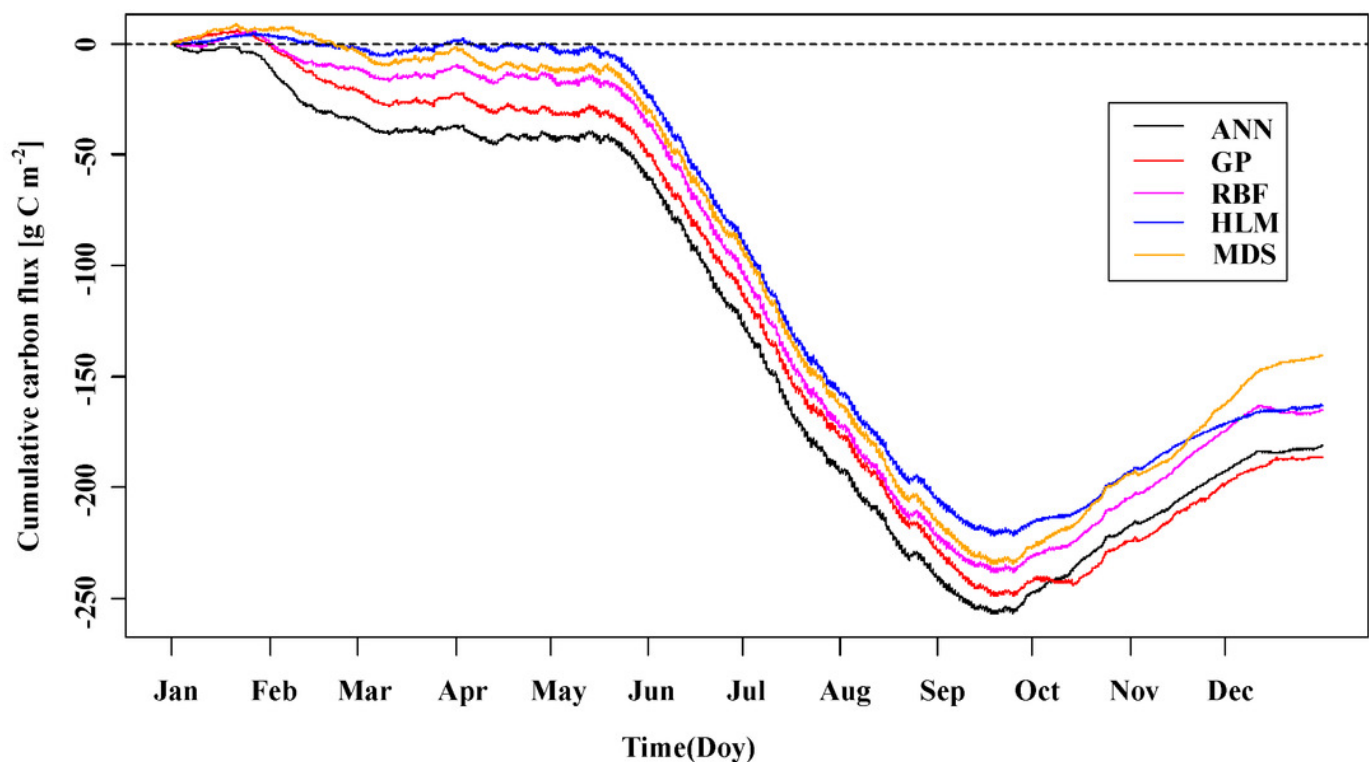
Data source of the driving factors and their corresponding pre-processing

Table 1. The data source of driving factors and their corresponding pre-processing

Variable	Name	Filled?	Pre-processing
Daytime	$hour_N$	No	Cos conversion to daily time.
Daytime	$hour_D$	No	Sin conversion to daily time.
Daytime	Night	No	Calculated the sunrise and sunset times at the observation area location and marked the data from post-sunset to pre-sunrise as nighttime.
Daytime	Day	No	Calculated the sunrise and sunset time at the observation area location and marked the data from post-sunrise to pre-sunset as daytime.
Season	$Season_G$	No	Marked the data from May–September as the growing season.
Season	$Season_N$	No	Marked data from January–April and October–December as the non-growing season.
Vegetation index	NDVI	Yes	NDVI from 250 m resolution MODIS/Aqua remote sensing image for 16 days
Air temperature	T_{air}	Yes	Measured at a height of 15 m on the flux tower.
Soil temperature	T_{soil}	Yes	Measured at a soil depth of 5 cm under the flux tower.
Water vapor partial pressure	E	Yes	Measured at a height of 15 m on the flux tower.
Heating degree days	hdd	Yes	When $T_{air} < 18°C$, equal to $18°C - T_{air}$; otherwise, equal to 0.
Incident radiation	Rd	Yes	The sum of incident shortwave radiation and incident longwave radiation measured by NR01, Campbell Scientific, USA.
Scattered radiation	Ru	Yes	The sum of scattered shortwave radiation and scattered longwave radiation measured by NR01, Campbell Scientific, USA.
Water vapor pressure deficit	VPD	Yes	Measured at a height of 15 m on the flux tower.
Relative humidity	Rh	Yes	Measured at a height of 15 m on the flux tower.

Quality control procedures for the 30-min flux data

Table 2. Procedures of quality control of the half-hourly flux data

Processing	The number of outliers		Description
	Growing season	Non-growing season	
Quality control	856	1021	Cleaning carbon flux data based on QC flags and removing values while QC flags equal to 2.
Distributional cleaning	679	464	Cleaning carbon flux data based on flux distribution for each hour of the day.
Filtering	62	26	Detecting and removing outliers in the continuous carbon flux data.
u^* screening	216	192	Cleaning carbon flux data based on friction vorticity threshold.

Standardized major axis estimation and statistical inference

1 **Table 3.** Standardized major axis estimation and statistical inference

Parameter	Non-growing season			Growing season		
	Estimate	Lower (2.5%)	Upper (97.5%)	Estimate	Lower (2.5%)	Upper (97.5%)
Elevation	-4.039e-3	-8.112e-3	3.399e-5	-0.011	-0.015	-0.006
Slope	0.095	0.094	0.097	0.106	0.104	0.107
H_0: variables uncorrelated.						
P-value	< 2.22e-16			< 2.22e-16		
R^2	0.730			0.706		
H_0: slopes are equal.						
P-value	< 2.22e-16					
Likelihood ratio statistic: 129.8 with 1 degrees of freedom						

Kendall's tau (τ) coefficient between the 5 different methods of carbon flux prediction and the corresponding residuals

Table 4. Kendall's tau (τ) coefficient between the four different methods of carbon flux prediction and corresponding residuals

Method	Non-growing season			Growing season		
	$DAY_{Rd<=400}$	$DAY_{Rd>400}$	NIGHT	$DAY_{Rd<=400}$	$DAY_{Rd>400}$	NIGHT
GP	0.148**	0.171**	0.221**	0.077**	0.145**	0.118**
RBF	0.048*	0.057	0.202**	-0.290**	0.082**	0.005
ANN	0.058**	0.005	0.134**	0.009	-0.009	-0.059**
HLM	0.079**	0.014	0.192**	-0.175**	0.033*	-0.060**
MDS	0.070***	0.071**	0.074**	0.182***	0.075***	0.012

Notes: *** indicates p-value < 0.01; ** indicates 0.01 < p-value < 0.05; * indicates 0.05 < p-value < 0.1.

Relationship between the magnitude of carbon flux and the standard deviation of random uncertainty

Table 5. Relationship between the magnitude of carbon flux and the standard deviation of random uncertainty

Method	Intercept (a)	Slope (b)	R^2
HLM	1.5477***	0.0579***	0.3191
ANN	1.4001***	0.0608***	0.3047
GP	1.3290***	0.1082***	0.5906
RBF	1.5208***	0.0777***	0.4190
MDS	1.5550***	0.1092***	0.4513

Notes: *** indicates p-value < 0.01; R^2 indicates the coefficient of determination.

Annual sum and deviation of the carbon dioxide exchange estimated by the different methods

Table 6. Annual sum and deviation of the carbon dioxide exchange estimated by the different methods

Gap-filling method	Annual sum of CO_2 exchange		Bias of Annual sum of CO_2 exchange		
	Mean	SD	Mean	Lower (2.5%)	Upper (97.5%)
ANN	-159.91	18.35	0.84	-9.55	10.73
GP	-178.25	8.01	11.22	1.37	21.71
RBF	-167.16	19.08	14.05	2.63	25.89
HLM	-156.95	3.15	-2.64	-14.65	9.55
MDS	-155.21	5.16	-13.69	-23.70	-4.20

Seasonal sum of carbon dioxide exchange estimated by the different methods

1   **Table 7.** Seasonal sum of carbon dioxide exchange estimated by the different methods

Method	Non-growing season			Growing season		
	Mean	Lower (2.5%)	Upper (97.5%)	Mean	Lower (2.5%)	Upper (97.5%)
GP	39.788	33.877	46.264	-220.245	-227.814	-212.417
RBF	68.292	62.380	74.767	-232.510	-240.080	-224.682
ANN	56.000	50.088	62.476	-216.624	-224.194	-208.796
HLM	61.033	55.121	67.508	-227.859	-235.428	-220.031
MDS	74.954	69.042	81.429	-229.959	-237.529	-222.131